iScience

CellPress
OPEN ACCESS

Article

The role of short-term and long-term water level and wave variability in coastal carbon budgets

Katherine N. Braun[1] and Ethan J. Theuerkauf[2,3,*]

SUMMARY

We investigated soil organic carbon dynamics at three freshwater coastal sites in the Laurentian Great Lakes using a simple carbon budget box model. Long-term carbon budgets (1939–2018) were developed using aerial photography and then compared to short-term carbon export (2018–2019) developed using drone data. This study puts forth a refined coastal carbon budget model that advances previous model iterations by: (1) examining spatial variability in carbon budgets, (2) including a temporally dynamic carbon inventory term, and (3) updating the erosional term. Half of the initial carbon stock of the combined sites was lost in the 80-year study period, which is severely imbalanced with the age of those coastal habitats (400–2000 cal years BP). Major periods of carbon loss corresponded to periods of elevated water level. Short-term loss of carbon during 2018–2019 corresponded to northeasterly extreme wave events during a period of above-average water level.

INTRODUCTION

Soil organic carbon (SOC) represents a significant component of the global carbon cycle (Lal, 2004; Smith, 2008); Beyond the utility of soil carbon fluxes for understanding broad scale Earth system processes, SOC dynamics are important to incorporate into land management decisions as conversion and degradation of habitat reduces economically and ecologically valuable soil carbon stocks (Smith, 2008). Additionally, SOC provides numerous benefits to soil health including stabilization of the soil matrix, storage of water, and provision of plant nutrient reservoirs (Lal, 2004; Milne et al., 2015). Quantification of the rates and processes of SOC fluxes is required in order to properly manage coastal systems with respect to ecosystem services.

Erosion of coastal habitats reduces SOC stocks as organic-rich soils are swept into marine and lacustrine environments (Braun et al., 2019; Pendleton et al., 2012; Theuerkauf and Rodriguez, 2017). A significant body of work has addressed the role of coastal erosion in the soil carbon dynamics of marine coasts both in temperate and cold-climate regions (e.g., Coverdale et al., 2014; Jorgenson and Brown, 2005; Vonk et al., 2012). Erosion of permafrost coasts in the Arctic has been shown to be a significant source of carbon to the Arctic seas (Grigoriev and Rachold, 2003; Jorgenson and Brown, 2005; Tanski et al, 2016, Tanski et al., 2019). Fritz et al. (2017) calculated that the contribution of carbon from eroding Arctic coasts is on the same order of magnitude as the flux from all Arctic rivers (Fritz et al., 2017). Saltmarshes contain large stores of soil carbon, but are rapidly losing area due to human activity, climate change, and coastal erosion (Hopkinson et al., 2012). Numerous studies have calculated the carbon budget of saltmarshes and found that rates of carbon loss are disproportionate to the time it took that carbon to accumulate (Coverdale et al., 2014; Sapkota and White, 2019; Theuerkauf et al., 2015; Theuerkauf and Rodriguez, 2017). Likewise, mangroves contain large stocks of carbon that are being lost due to land conversion and sea level rise (Atwood et al., 2017; Donato et al., 2011; Kauffman et al., 2011; Pendleton et al., 2012). In all of these coastal environments, erosion plays a critical role in both exporting once stored carbon and reducing the area of coastal habitats available for carbon storage.

The connection between coastal erosion and carbon budgets of large lacustrine systems such as the Laurentian Great Lakes is poorly understood, although these systems experience high rates of coastal erosion similar to marine and estuarine coasts (Kimball May et al., 1983; Meadows et al., 1997). Coastal erosion is a significant problem in the Great Lakes as it destroys infrastructure and property (Angel, 1995) as well as

[1]Illinois State Geological Survey, Prairie Research Institute, University of Illinois at Urbana-Champaign, Urbana-Champaign, IL 61820, USA

[2]Department of Geography, Environment, and Spatial Sciences, Michigan State University, East Lansing, MI 48824, USA

[3]Lead contact

*Correspondence: theuerk5@msu.edu

https://doi.org/10.1016/j.isci.2021.102382

natural habitat, parks, and recreational areas, many of which contain important carbon-storing habitats such as coastal wetlands. Along Lake Michigan alone, 22% of the shoreline is classified as open-shore wetlands (Office of Coastal Management, 2020, https://www.fisheries.noaa.gov/inport/item/59439), which are vulnerable to erosional loss (e.g. Braun et al., 2019). Great Lakes coastlines provide numerous ecosystem services, including sport fishing, boating, and recreational use (Allan et al., 2015), in addition to the economic and ecologic value of the SOC stored within shoreline habitats. The total quantity of SOC lost due to coastal erosion in the Great Lakes is unknown, however, previous studies in the region suggest that the losses are episodic in response to storm events and high water levels and that carbon is being lost on orders of magnitude shorter timescales than the amount of time it took to accumulate that carbon (Braun et al., 2019). These losses will lead to a permanent reduction in the carbon stock through time if carbon accumulation rates do not increase to balance export or if habitat lost is not balanced by gain in new habitat area.

The episodic nature of SOC budgets in the Great Lakes in response to storms and water level fluctuations necessitates the use of a geomorphic process-driven SOC budget model to explore carbon dynamics through time. While a few studies have examined SOC in Great Lakes coastal wetlands (Bernal and Mitsch, 2008; Braun et al, 2019, 2020), no studies exist exploring SOC dynamics beyond wetland habitats in the region. This represents an important gap in documenting regional SOC budgets as a large portion of the coastal habitats in the Great Lakes region are not wetlands, but rather other SOC-containing environments, such as prairies and savannas. Additionally, these studies do not model carbon storage using a temporally dynamic carbon inventory term nor allow for alongshore variability in the area of SOC-containing habitats through time. In order to address these gaps and improve our understanding of the temporal and spatial dynamics of coastal SOC budgets, we modified the Braun et al. (2019) model to: (1) incorporate spatial variability in carbon storage and areal change in various coastal habitats, (2) include a temporally dynamic carbon inventory term, and (3) enhance the capabilities of the model to realistically capture the dynamics of coastal erosion and SOC export (full model details are presented in the transparent methods, also see Figure S2).

We use this model to evaluate changes in SOC budgets from 1939 to 2019 at a 2.75 km stretch of shoreline along western Lake Michigan that exhibits a high degree of spatial and temporal variability in shoreline retreat rates, SOC storage rates, and coastal habitat types. Illinois Beach State Park (IBSP) is a 1,680-hectare park situation on the Zion Beach-ridge Plain along the shore of Lake Michigan in northeastern Illinois, USA (Figure 1). The Zion Beach-ridge Plain is a dynamic sand body composed of curvilinear beach ridges and swales. This ~3,700-year-old landscape is dominated by erosion along the northern two-thirds of the park and accretion along the southern third due to the predominantly north to south longshore current (Chrzastowski et al., 1994). Waves and fluctuating water levels are the dominant hydrodynamic processes that generate change and ultimately alter SOC budgets along most coastal environments. In the Great Lakes, water levels fluctuate dramatically across a range of timescales from storm events to millennia (As-Salek and Schwab, 2004; Gronewold and Rood, 2019; Thompson and Baedke, 1997). On timescales relevant to management (seasonal, annual, decadal), Lake Michigan fluctuates in a ~2 m range, with the long-term average water level at 176.606 m NAVD88 (Figure 2).

The updated SOC budget model is flexible; it can be applied over large and small spatial and temporal scales to identify trends in SOC, in addition to identifying carbon budget responses to events such as storms or fluctuations in water level. Given this, it can provide important data on SOC dynamics in coastal systems that can be used for management of all SOC-containing shoreline habitats, not just wetlands or those within the Great Lakes region. Additionally, this model allows land managers of any coastal setting to pinpoint areas of high value and vulnerability by identifying hot spots of carbon accumulation and loss.

RESULTS

Coastal habitat area significantly declined over the past 80 years

Carbon storage and export is calculated based on the area of habitat present or eroded. The rate of change in areal extent of habitat for the entire study period and area was −3,569 m^2/year, or −1.3 m^2/year per meter of shoreline. The rate of habitat area change for the long-term record, 1939 to 2018, was −4,423 m^2/year (−1.6 m^2/year per meter of shoreline); the rate for the short-term record, 2018–2019, was −13,101 m^2/year (−4.8 m^2/year per meter of shoreline). The rate of habitat area change in the long-term record was positive only during the record low water levels of the late 1990s and early 2000s, between 1997 and 2000, 2002–2004, and 2007–2008. In the short-term record, the rate of habitat change was positive during the summer

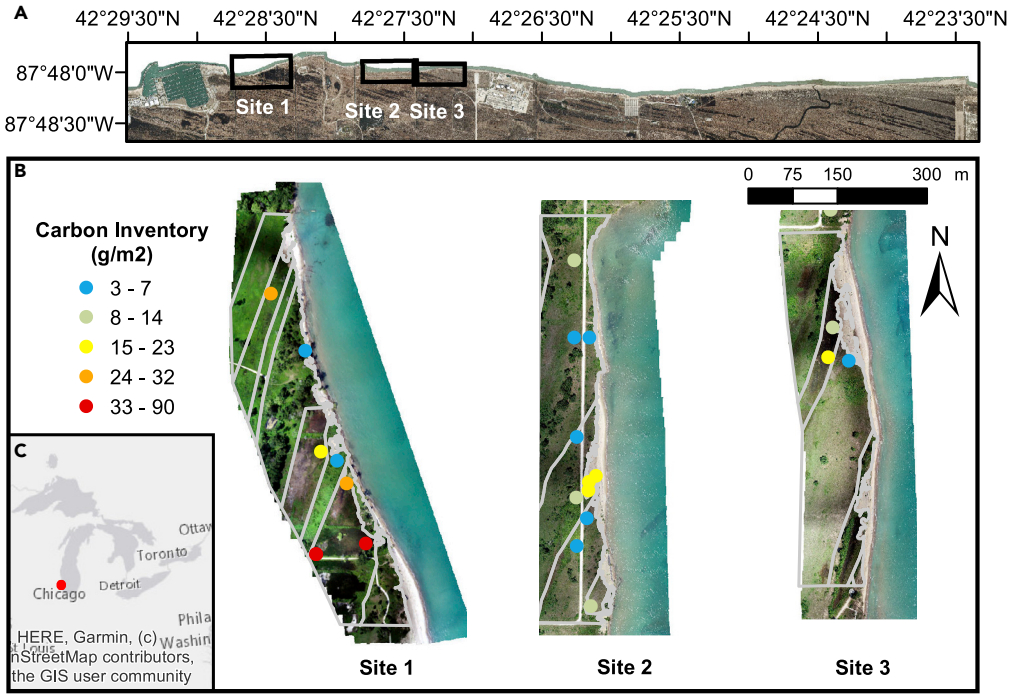

Figure 1. The three study sites are located along the southwestern shore of Lake Michigan, Illinois, USA

(A) Location of the three study sites along the North Unit of Illinois Beach State Park.

(B) sUAS-derived orthomosaics of the three study sites. Gray boundaries mark the habitat areas. Circles indicate coring locations and are color-coded to show the carbon inventory of each core.

(C) Location of study area in United States of America. Aerial image in panel a downloaded from the Lake County, Illinois Planning, Building, and Development Department.

See also Figure S3 and Table S1.

growing season of 2019, between April 25 and June 17, 2019, and July 10-26, 2019. During periods of habitat loss, the average rate of loss was −14,098 m^2/year; during periods of habitat gain, the average rate was 2,824 m^2/year, which highlights the order of magnitude difference between the formation and destruction of habitats and associated carbon storage.

The highest rates of habitat change seen during the study period occurred during the short-term, high-resolution record. This is likely in part due to near record high lake levels, but also due to the increased fidelity of the record. It is likely that during other erosional periods in the past similarly high rates of loss would have been documented. The highest rate of change was −48,890 m^2/year (−17.8 m^2/year per meter of shoreline), between August 31 and September 11, 2018. Other periods of high magnitude habitat loss include 2017–2018 (−24,336 m^2/year; −8.8 m^2/year per meter of shoreline), October 24-November 5, 2018 (−36,274 m^2/year; −13.2 m^2/year per meter of shoreline), November 5-December 18, 2018 (−43,865 m^2/year; −16.0 m^2/year per meter of shoreline), and March 28-April 25, 2019 (−41,947 m^2/year; −15.3 m^2/year per meter of shoreline).

Coastal habitats lost an order of magnitude more SOC than was stored in 80 years

All three study sites lost more carbon than they stored over the long-term study period, from 1939 to July 26, 2019. Combined carbon export by erosion at all sites (1939 area: 0.56 km^2; 2019 area: 0.20 km^2) over the entire study period was 4,420 MgC, while combined carbon storage was 579 MgC. We define carbon export as the product of the amount of soil carbon contained per unit area and area of habitat eroded; carbon storage is the product of the carbon accumulation rate and the total amount of active habitat (see transparent methods for model details). Given the imbalance between carbon stored and carbon exported, these sites collectively are carbon sources on decadal timescales. The carbon stock for the entire study area decreased over the 80-year period, from a total of 7,504 MgC to 3,663 McC, a loss of 51% of the

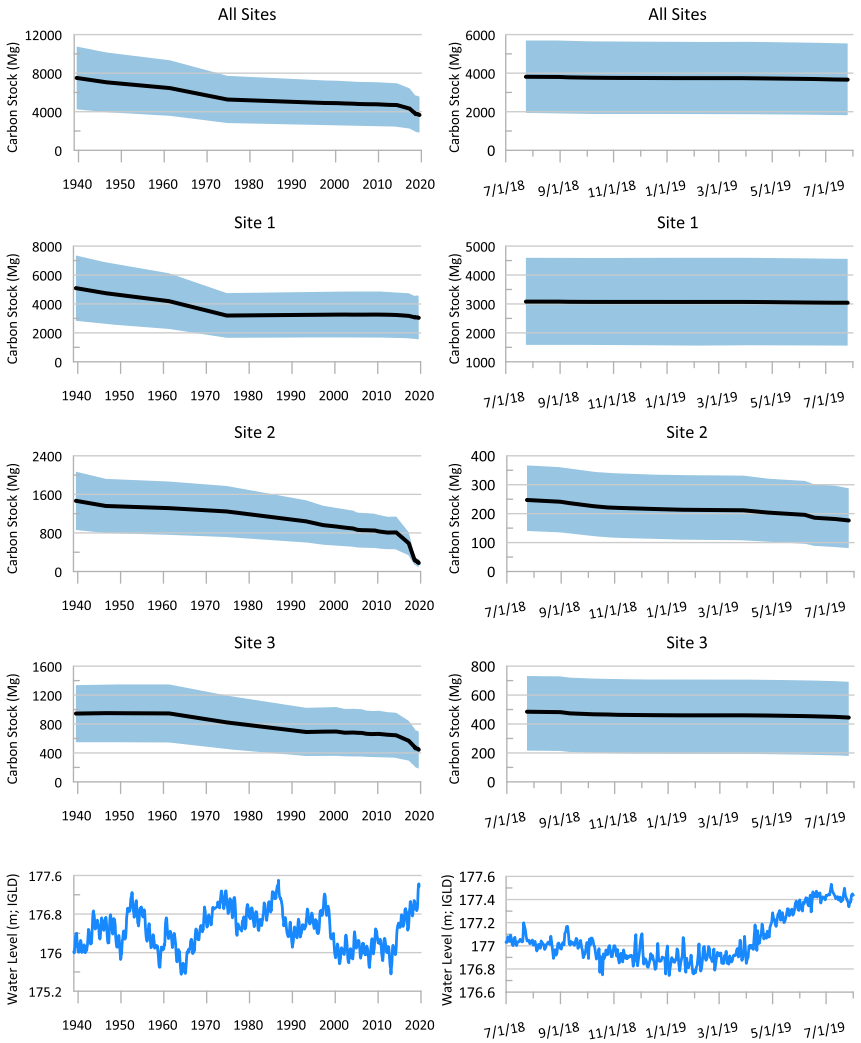

Figure 2. The greatest loss in carbon stock occurs during intervals of water level rise

Plots depicting the change in carbon stock and change in the water level of Lake Michigan from 1939 to 2019 (left) and the short-term monitoring record from 2018 to 2019 (right). Shaded blue indicates error of the carbon stock, measured using high and low values for the carbon inventory, wetland age, and geospatial analysis. See also Figure S2 and Table S2.

initial stock (Figure 2); this amount is a carbon budget rate of −0.09 kgC/m^2/year (Figure 5). Examining the site-specific budgets allows for a more detailed analysis of the variability in SOC dynamics as they relate to geomorphic change and habitat type.

All study sites were carbon sources throughout most of the 80-year record, however, there was substantial temporal and spatial variability in the magnitude of carbon storage and export. Site 1 lost the most carbon of all the sites, 2,322 MgC, which is a carbon budget rate of −0.12 kgC/m^2/year. Site 2 lost the highest percentage of its original stock, 88%, which was 1,463 MgC; this site has a carbon budget rate of −0.07 kgC/m^2/year. Site 3 lost the least carbon, 635 MgC, which is a carbon budget rate of −0.06 kgC/m^2/year. While the sites all lost more carbon than was stored over the entire 80-year study, during some time-steps individual sites stored more carbon than was exported. The 2008–2009 period is the only time when the total carbon budget of all sites combined was positive. The carbon stock increased 0.02% during 2008–2009 as 1.66 MgC was gained between all three sites. Site 1 had a positive carbon budget between: 1974–2002, 2004–2005, and 2006–2009. Site 2 only had a positive carbon budget in 2012–2014. Site 3 had a positive carbon budget between 1939 and 1946, 1993–2000, 2002–2004, and 2008–2010. Even though there were times in this study when a given site had a positive budget, the fact

that the other sites had negative carbon budgets during that same time offset any gains when considering the whole study area. For example, combining all of these periods of positive carbon budgets together, these sites had a cumulative carbon budget of 97 MgC, which is an increase of 1% in the carbon stock. During these same periods at the other sites with negative carbon budgets, 1,069 MgC was lost, which is a decrease of 14% in the carbon stock. This offset between carbon gain and loss across the sites can also be observed at discrete time intervals. For example, though site 1 gained 47 MgC between 1974 and 1993, site 2 and site 3 lost 339 MgC in that same period.

The cumulative amounts of carbon exported and stored at each site were plotted against each other to illustrate the relationship between these two fluxes over the decadal record (Figure 3). While the carbon budget was occasionally positive, the cumulative amount of carbon exported was always greater than the cumulative amount of carbon stored, except at site 3 between 1939 and 1961. Habitat at site 3 during this period migrated lakeward due to colonization of the wide sandy beach that had been previously present, allowing the site to accumulate more carbon than was exported during this time. The cumulative amount of carbon exported from all sites during the study period is 7.6 times greater than the cumulative amount of carbon stored.

High water level and increased wave heights align with high carbon export events

Lake Michigan water level data were analyzed for the entire study period and compared with the carbon budget dynamics. The greatest loss in the carbon stock at these sites in the long-term record is seen during periods when water level rises. The largest increase in Lake Michigan water level, +2.1 m, occurs between 1961 and 1974 when the carbon stock dropped by the largest percent, 16%. A similar pattern appears in the data for the most recent rise in water level, between 2014 and 2019: water level gained +1.5 m, while the carbon stock decreased by 14%. The sites lost 8% of the carbon stock in 1946–1961, during a +1.6 m rise in water level. A decrease in the carbon stock during the record highs of the 1980s is seen at sites 2 and 3, but not at site 1, which received sediment nourishment from the construction of North Point Marina (completed in 1989). The carbon stock of all sites decreased 2% during the record low water levels of the early 2000s (2000–2012).

No major increase in carbon storage nor recovery of the carbon stock appears to occur when water level falls. The only time-step we analyzed that fully encompasses a fall in water level is 1997–2000, when water level peaked at 177.30 m IGLD in July 1997, and reached a low of 175.75 m IGLD in December 1999, a fall of 1.55 m. At all sites during this time, the carbon budget is negative; this indicates that although the water level was falling to near record lows, carbon was still being exported more than it was stored. In other time-steps with major decreases in water level (1946–1961, 1961–1974, and 1974–1993), any gain in carbon storage during falling water levels was outweighed by the amount of carbon lost through erosion during subsequent time periods (Figure 3).

The high-resolution 2018–2019 record shows that seasonal trends in carbon loss at the study sites are controlled by water level and wave dynamics. Carbon export is reduced in the winter months and increases during the spring, summer, and fall seasons (Figure 3). At all three sites, carbon export leveled off around October-November 2018, as water level fell ~0.15 m from the summer 2018 high, and then export began to increase again in March 2019 as water level rose ~0.55 m.

Wave data for the 2018–2019 short-term record were also compared to the carbon export rate. The average significant wave height for the short-term record was 0.42 m; the 98th percentile of significant wave height was 1.31 m. The time-steps with the greatest percentage of extreme waves (>98th percentile) were August 31, 2018-September 11, 2018 (13%), October 24, 2018-November 5, 2018 (5.4%), November 5, 2018-December 18, 2018 (5.3%), and March 28, 2019-April 25, 2019 (5.0%). Rose diagrams of wave direction were also produced (Figure 4).

Extreme wave events align with periods of high carbon export and habitat loss. High rates of carbon export and habitat loss between August 31, 2018 and September 11, 2018 occurred during a large wave event. A similar pattern appears between March 28, 2019 and April 25, 2019. While there are few extreme wave events following April 25, 2019, both the carbon export rate and habitat change rate remain elevated, which tracks the seasonal rise in water level during the spring. There is a similar percentage of extreme wave events between October 24, 2018 and December 18, 2018 as during the spring 2019 storm season, but little carbon export occurs during this time. Wave direction differs between these two periods

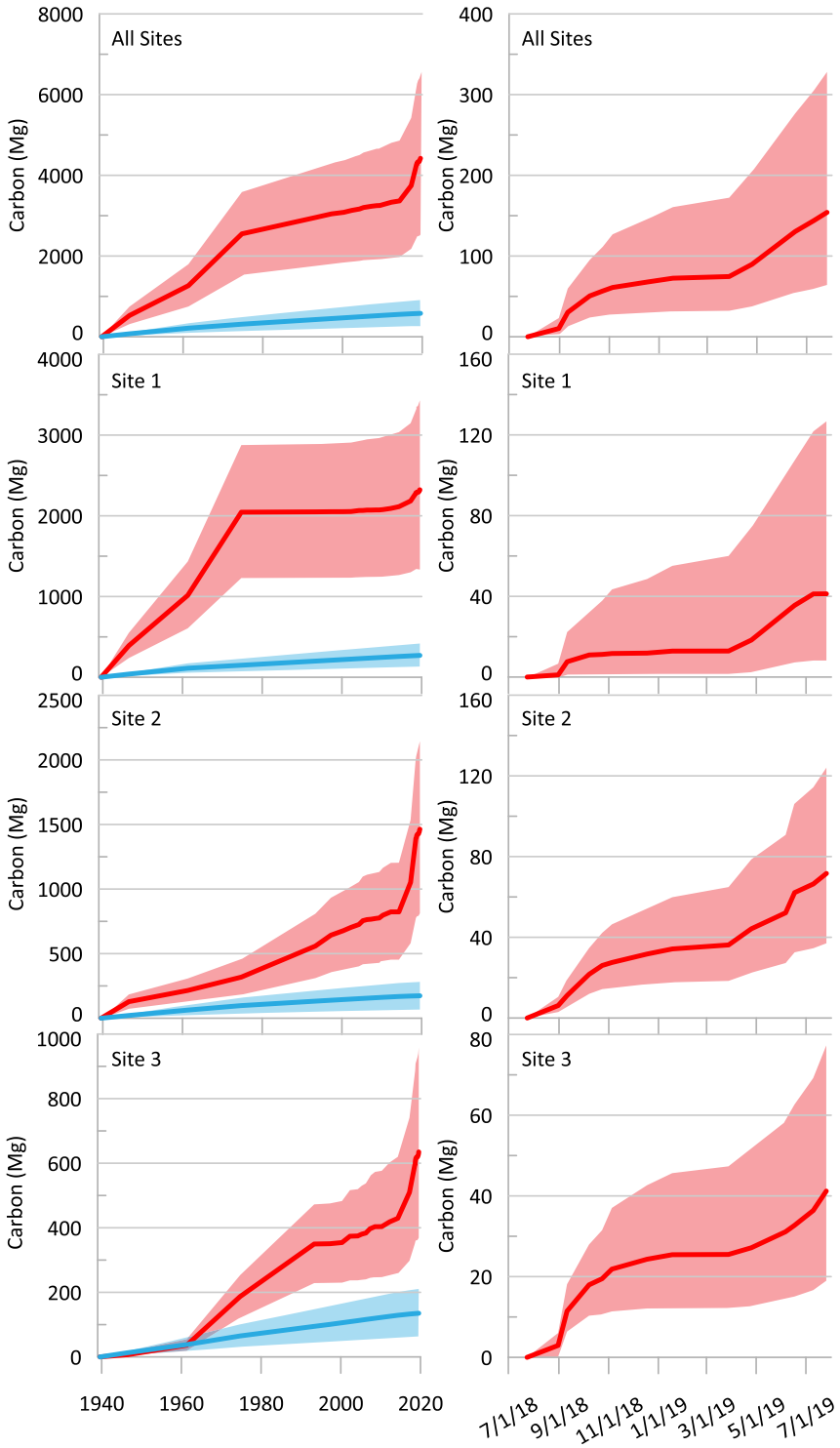

Figure 3. Cumulative carbon export exceeds carbon storage by seven times

The red line indicates the total amount of carbon exported. The blue line indicates total amount of carbon stored. Shading indicates error of the carbon stored and exported, measured using high and low values for the carbon inventory, wetland age, and geospatial analysis. See also Figure S2 and Table S2.

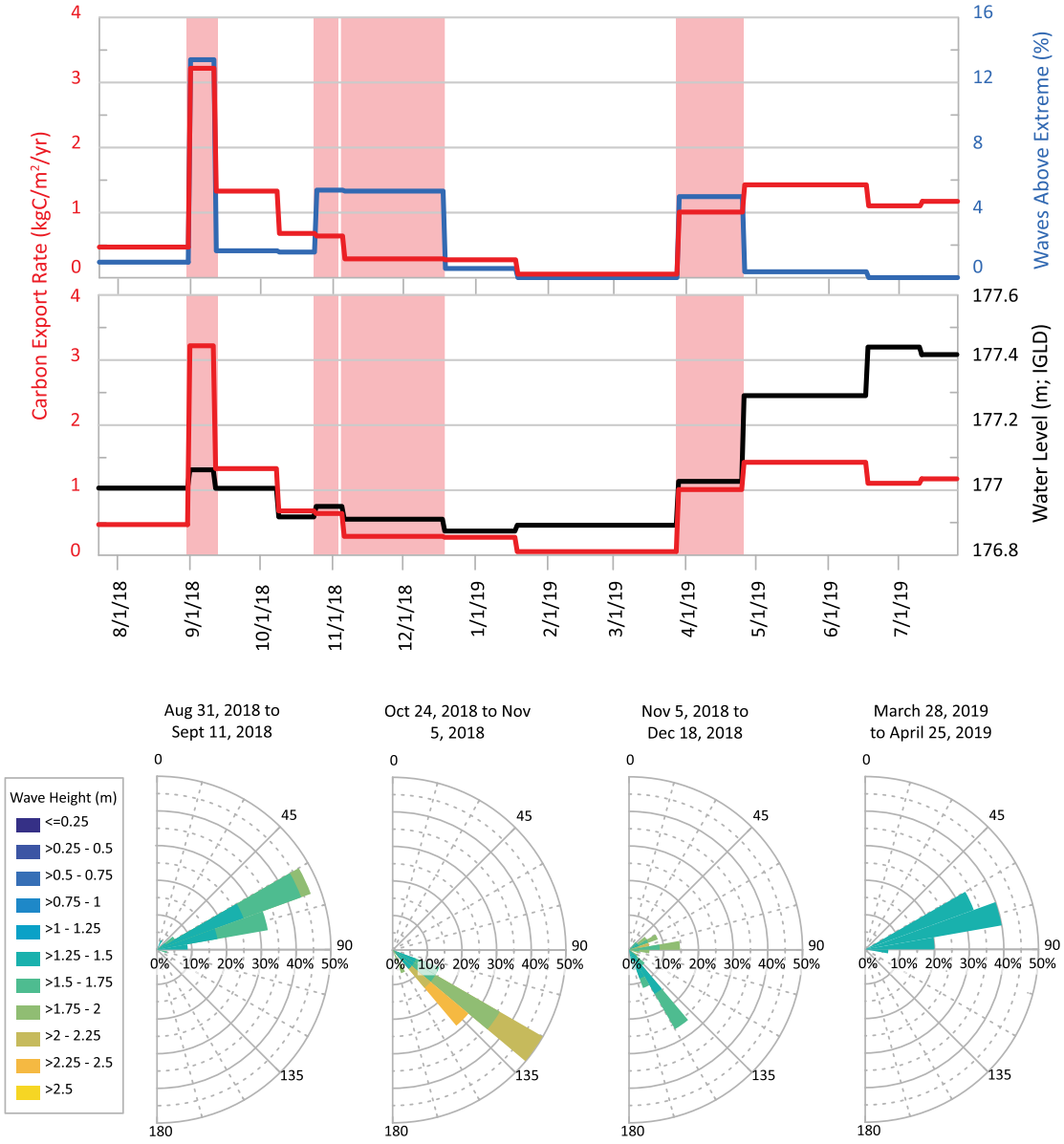

Figure 4. The greatest export of carbon occurs during northeasterly extreme wave events

Top: carbon export rate (red) and percentage of waves above the extreme threshold (98th percentile of all waves; in blue), with red shading indicating periods that have wave rose charts depicted below. Middle: carbon export rate (red) and average water level (black), with red shading indicating periods that have wave rose charts depicted below. Bottom: Wave rose charts showing the extreme onshore wave events for each highlighted time bin.

(Figure 4). During the spring stormy period, onshore waves come primarily from the east, with an average direction of extreme waves of 75°. In the fall 2018 storms, wave direction is more southerly, with an average direction of extreme waves of 130° in October 24, 2018 – November 5, 2018, and 115° in November 5, 2018 – December 18, 2018. While the carbon export rate lowered during the fall 2018 storms, the habitat area change rate remained elevated due to enhanced overwash burial of habitat. The sUAS imagery during this period reveals sustained growth of washover fans in response to the fall 2018 storms.

DISCUSSION

Carbon loss through time

Coastal habitats at this study area lost seven times the amount of carbon they stored over the past 80 years. This imbalance between carbon export and carbon storage makes all of these sites carbon sources rather

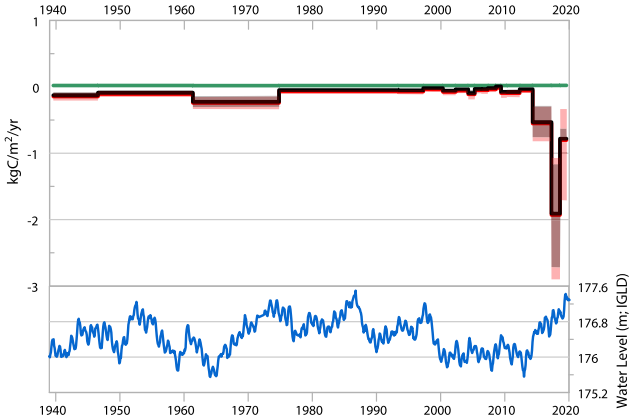

Figure 5. The 80-year carbon budget is negative

Top: carbon storage rate (green), carbon export rate (red), and carbon budget rate (black) for the decadal record, 1939–2019. Error represented by shaded areas. Bottom: water level.

than carbon sinks across decadal timescales. Without considering the coastal geomorphic processes that are at work, the carbon dynamics of these habitats cannot be evaluated accurately and they would likely erroneously be considered carbon sinks given the mere presence of wetlands and other habitats known for their carbon-containing soils. The carbon stock at the three study sites diminished from 7,504 MgC to 3,663 MgC between 1939 and July 2019, a rate of loss of −0.09 MgC/m^2/year (Figures 2 and 5).

This study only documented carbon dynamics along a 2.75 km stretch of shoreline, while the Great Lakes as a whole has over 16,000 km of shoreline. Not all sections of the Great Lakes shoreline are composed of the same habitats as IBSP nor do all stretches of coastline erode at the same rates. However, estimates indicate that 85% of the total Great Lakes shoreline is not hardened and that long-term retreat rates are on average −0.7 m/year, which potentially puts coastal habitats at risk of eroding (Kimball May et al., 1983; Schneider et al., 2007). If we combine these data with the carbon inventory of the least carbon-rich habitat at our study sites, mesic sand prairie, we estimate that the Great Lakes region has lost ~5.1 TgC from coastal habitats over the past 80 years. Given the lack of data on Great Lakes coastal soil carbon content and erosion rates, this estimate is not meant to be taken as an exact value but rather highlights the significant role coastal erosion in the Great Lakes plays in carbon cycling. From the results of our study and others, coastal erosion clearly has the potential to generate significant fluxes of carbon and associated economic and ecologic impacts.

Carbon is lost from coastal habitats through shoreline erosion when coastal processes, such as storm waves or fluctuating water levels, erode these SOC-containing environments. While studies have examined the erosional loss of coastal soil carbon (Ganju et al., 2019; Sapkota and White, 2019) and the global impact of that carbon loss (Pendleton et al., 2012), the pathways and degradation of coastal SOC are complex and not completely quantified (Spivak et al., 2019). Depending on physical and biogeochemical conditions, the carbon may be remineralized and respired as atmospheric CO_2 or redeposited in other carbon pools (Hayes et al., 2021; Sapkota and White, 2021; Tranvik et al., 2009) No matter the fate of this eroded carbon, it is no longer stored in the coastal ecosystems where it originated, thus, natural resource managers must critically evaluate whether a site truly is a carbon sink based on the dominant geomorphic processes. The long-term erosional trend at IBSP indicates that coastal ecosystems and associated carbon lost is permanent; over decadal time periods the land and carbon lost is not regained, even during periods of low water levels. Therefore, carbon storage as well as other ecosystem services associated with the eroded habitat are permanently lost during these high water level periods, which necessitates revaluation of whether a given site should be prioritized for shoreline protection due to habitat conservation needs or whether managed retreat should be allowed.

Hydrodynamics

The previous version of this carbon budget model published in Braun et al. (2019) identified short-term impacts of storm events and seasonal water level fluctuations on carbon budgets in coastal wetlands.

However, that model did not contain the complexity necessary to evaluate the processes influencing coastal carbon budgets over larger temporal and spatial scales. A broader spatial and temporal context is required to evaluate the role that long-term water level fluctuations play on coastal habitat loss as well as carbon budgets. The expansion of the Braun et al. (2019) model to include a longer timescale, a broader spatial context, a refined carbon export term, and a temporally dynamic carbon inventory term allows us to identify what conditions during the past century led to carbon loss at these sites. This framework can be extrapolated to sites throughout the Great Lakes region as well as globally to assist coastal managers in identifying shoreline areas that are vulnerable to carbon loss on a range of timescales.

Carbon loss at our study sites generally tracks annual and decadal fluctuations in Lake Michigan water levels. Carbon export rates at all sites and time frames (short and long-term) in this study occurred jointly with increasing water level (Figure 5). While saltmarshes tend to experience reduced erosion rates when high water level leads to waves breaking across the marsh platform rather than at the marsh edge (Tonelli et al., 2010; Valentine and Mariotti, 2019), Great Lakes coastal habitats experience increased edge erosion rates during periods of higher water level (Angel, 1995; Meadows et al., 1997; Theuerkauf et al., 2019). Higher water levels amplify the impacts of waves and storms as energy is consistently delivered at higher elevations on the shore profile and therefore can reach larger portions of coastal habitat and soil. Thus, increased export of carbon can occur even during periods with low-magnitude shifts in water level when the base water level is high and wave energy is driven farther up the shoreface.

The high-resolution 2018–2019 data set allows us to examine linkages between hydrodynamics and carbon export on a monthly scale. These data show that carbon is exported during periods with high water level and northeasterly extreme wave events (Figure 4). The short-term record contains three periods with extreme waves, August-September 2018, October-December 2018, and March-April 2019. The October-December 2018 events did not cause similar levels of carbon export as the other two events, even though the late fall storms had maximum wave heights 0.58 m (30%) higher than the other events. These late fall storm events differed from the other storms in two ways: water level was over 0.10 m lower than the other events, and the waves originated from a more southerly direction which generates less erosion than northerly waves given the shoreline geometry of IBSP. It is the combination of these two factors that attenuated the impact of these storms on coastal carbon export. Although the majority of the waves during this period were south to southeasterly, the November 5, 2018 – December 18, 2018 period saw 40% of the extreme waves originate from the northeast to east. These easterly extreme waves, however, did not cause the extensive carbon export that similar waves did during the September 2018 and April 2019 events likely due to the lower water level in the late fall. Wave energy from this event was reaching portions of the shoreface that had already eroded during the event in September 2018. The high-resolution short-term record reveals that large carbon export events occur during extreme wave events when water level is elevated. These findings reiterate the importance of annual fluctuations in water level to coastal habitats and carbon budgets.

Although storm events and anthropogenic modification impact carbon export on shorter timescales, such as the storm around September 7th, 2018 or the construction of North Point Marina in the late 1980s, on longer timescales it is the annual and decadal fluctuations in water level that impact the areal extent of coastal habitats and therefore the carbon budgets. As the extreme wave events in the short-term record revealed, high water level enhances the erosional impact of a storm event. Water level is the driver of major coastal erosion and carbon loss, and this relationship should be taken into account when planning long-term management of Great Lakes coastal sites like IBSP.

The Braun et al. (2019) carbon budget model showed that wetland carbon budgets at IBSP are controlled primarily by erosional events and that the reduction in carbon storage potential by overwash played a relatively minor role in reducing carbon storage compared to erosion. Over the longer time frame examined in this study we found further evidence of this trend. The amount of carbon exported from shoreline habitats over the 80-year study period was seven times larger than the amount of carbon stored. Any reduction in carbon storage due to overwash is outweighed by the larger impact of erosion and associated carbon export on the carbon stock (Figure 3). Given the influence of erosion on decadal carbon budgets, it also appears that any growth of vegetation on washover deposits has only a minimal positive impact on overall carbon budgets.

While all sites experienced carbon loss during periods of high water level, the impact of the high water levels in the 1980s on the carbon stock is less than other periods of high water level. This response is unexpected given the dramatic erosion that was documented throughout the Lake Michigan basin during this period (Angel, 1995; Meadows et al., 1997). The attenuated impact on carbon stocks during this period is likely due to the effects of updrift human disturbance associated with the construction of North Point Marina in the late 1980s. During and following the construction of North Point Marina, erosion of fill material, as well as the placement of excess sand led to artificial nourishment of the beach area south of the marina (Chrzastowski et al., 1996), which is the northern boundary of site 1. The lack of change in the carbon stock between 1974 and 1993 at site 1 is likely due to the pulse of new sand into the littoral system in the late 1980s, as it would have protected the shoreline during the years of high water level. The period between 1974 and 1993 includes the fall from the high water level of the mid-seventies, the rise to the 1986 record, the fall to a low in 1990, and a gradual rise following that low. Additional aerial imagery of the intervening years between 1974 and 1993 would allow for a more detailed evaluation of the interplay between high water levels, anthropogenic influence, and shoreline habitat change; however, the limited habitat loss and carbon export documented across this entire period suggests that the longer-term impacts of this human disturbance overwhelms any shorter-term erosion that may have occurred during peak water levels.

Carbon budget model updates

The updated model presented in this manuscript evaluates the capacity of a coastal site to store carbon in different habitat types over long temporal scales. The updated carbon export term more realistically reflects the process of carbon loss due to erosional ravinement on the shoreface by using 3D topographic data. The use of spatially averaged carbon accumulation rates and carbon inventories as inputs allows application of the model across larger spatial scales and accounts for heterogeneity within study sites. The temporally dynamic carbon inventory term allows use of the model across decadal timescales. Finally, the parameterization of the model using geospatial data acquired from aerial images reflects the shift toward UAS-data collection in coastal systems (Johnston, 2018) and supports the use of publicly available satellite and aerial imagery data sets to parameterize the model rather than relying on site-specific field data.

The expansion of the model from a wetland-focus to a more holistic landscape focus allows users to examine carbon dynamics across wider areas that are more relevant to management. As this model is suitable for use across broader spatial scales, it can be used to document linkages between coastal processes, landscape impacts, and carbon budgets. For example, the areas in this study site with the most rapid change and greatest loss of carbon align with high-risk areas for coastal erosion defined in Theuerkauf et al. (2019). Site 2 is immediately downdrift of a hardened shoreline and experienced the greatest loss in land over the 80-year study period (17 hectares, 74% of initial area), and in percent of stock lost (88%, 1463 MgC).

Applications for coastal management

The rate at which carbon is exported from these coastal sites is not in balance with the amount of time it took to accumulate these stocks of carbon. The base of the soil organic unit at site 1 was dated to 1934 cal years BP in the north of the site, and 830 cal years BP in the south; sites 2 and 3 were dated to 394 cal years BP. Half of the carbon stored in the three study sites was lost in 80 years, an order of magnitude faster than the shortest amount of time it took to form these carbon stocks. Additional stocks of soil carbon exist in other habitats at IBSP beyond the areal extent of this study, both along the rest of the shoreline at IBSP as well as landward of the study sites. We documented 36 hectares of coastal habitat lost at the three study sites in 1939–2019; this loss represents 2% of the 1680 hectares of IBSP, not taking into account erosion occurring along the 7.75 km of shoreline not included in this study. While coastal erosion and habitat loss is a known concern for coastal managers throughout the Great Lakes region, little has been done historically beyond site-specific shore protection to manage the issue of coastal habitat loss, in part due to the difficulty of deciding where to devote limited resources. Our study provides context on the value of different coastal habitats through the lens of carbon storage, which can be used to prioritize shoreline protection efforts in the context of habitat conservation. The results of our carbon budget show that managers must be accounting for soil carbon loss in coastal systems and cannot assume that these habitats contain sustained carbon pools without examining carbon loss due to erosion.

At our study site, high carbon value areas are located at sites 1 and 3. We define high carbon value as locations with carbon inventories and/or carbon accumulation rates that are high relative to the average

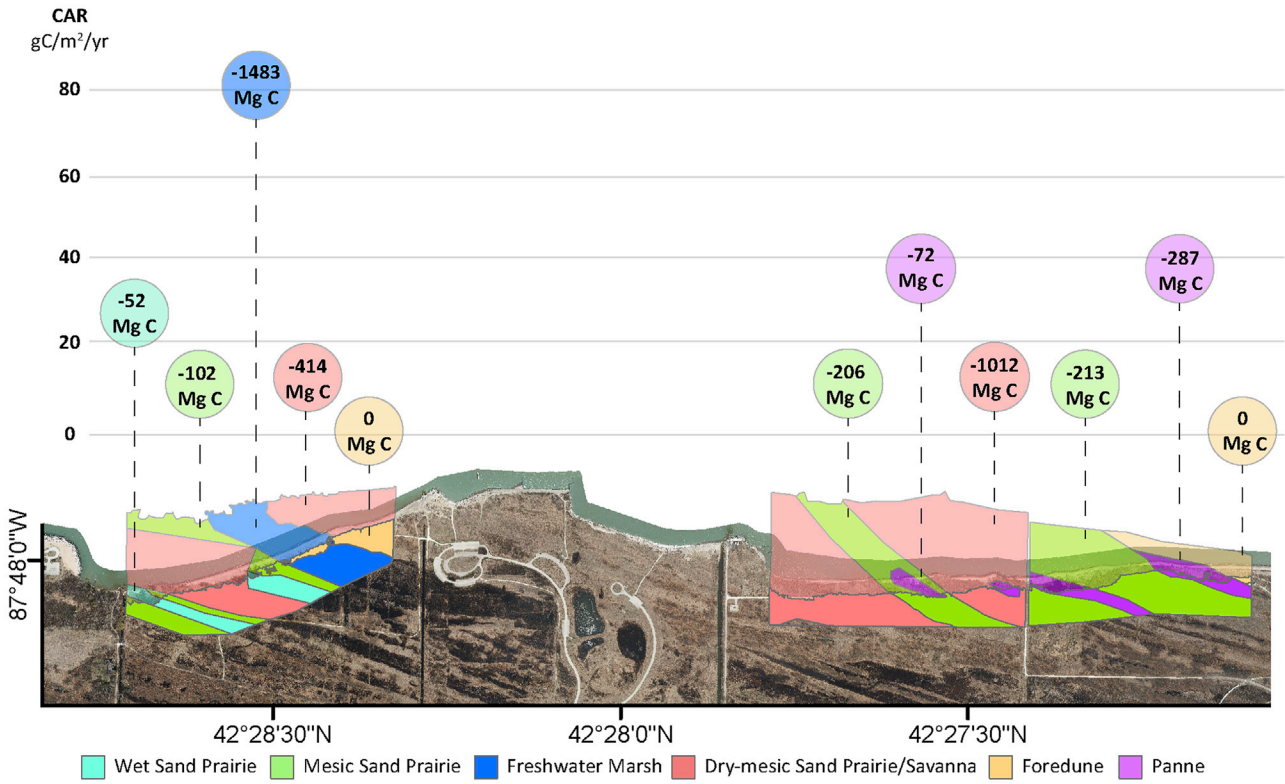

Figure 6. Eighty years of coastal habitat and carbon loss

Total habitat area lost between 1939 and 2019, with bubbles indicating the loss in carbon stock during that period in each habitat type for each site. The height of the bubble corresponds to the average carbon accumulation rate for that habitat type. Aerial image is from 2017, downloaded from the Lake County, Illinois Planning, Building, and Development Department. See also Tables S4–S10.

values (Figure 6). Habitats with high carbon inventories have large stocks of soil carbon, while habitats with high carbon accumulation rates are able to store carbon faster and therefore recover faster from erosive events. Freshwater marsh and wet sand prairie are the two habitat types in this study with the highest carbon inventories (73,565 and 45,163 gC/m^2 respectively). Freshwater marsh, panne, and wet sand prairie have the highest carbon accumulation rates (82, 38, and 27 gC/m^2/year respectively). While site 2 contains high value pannes, those pannes lost almost all of their original extent by the end of the study period. Given the minimal area left of panne at this site, as well as the likelihood that the loss is permanent given the trends in historical habitat loss in the area, this site would not be an ideal location for conservation efforts if carbon storage is the management priority. Site 1 contains a large freshwater marsh that began to fill in with washover sediment during the 2018-2019 study period yet remained relatively intact by the end of the study. Site 3 contains large, intact panne habitats along the shoreline that were eroding and filling with washover sediment during the study period. Shoreline protection measures should focus on the high value wet sand prairies and freshwater marsh at site 1 and the pannes at site 3 in order to conserve the carbon stock and storage potential of these habitats.

Limitations of the study

Study results are limited by the errors and assumptions of the carbon budget model and its inputs. Model error, represented in figures by shading, was determined by running the model with the high and low values for the carbon inventory (standard deviation; Table S4), carbon accumulation rates (radiocarbon date error; Table S4), and geospatial data (see transparent methods). Averaging carbon inventories across habitat types obscures some small-scale (100s m^2) variation in carbon inventory in favor of creating a carbon inventory that is acceptable for use across the entire study sites (1000s-10,000s m^2). The use of a static carbon accumulation rate assumes that carbon storage in these habitats is linear over decadal timescales, when seasonality is known to cause variations in the carbon accumulation rates in temperate locations. Defining

precise boundaries between habitat types over decades introduces error as landscapes evolve and such hard boundaries do not exist in natural settings; this factor was attenuated by manual editing of boundaries when such differences were clearly visible on historical photographs.

Assessing carbon budgets at different scales requires different levels of data. Larger regional budgets make greater assumptions about spatial heterogeneity in carbon stocks in order to track larger-scale patterns; our parameterization of the carbon budget at three relatively small sites allowed us to address the variability in carbon dynamics between different habitats. Site-level studies, such as this one, can capture precise relationships between processes and responses that can later be applied at greater scales; carbon-content data collected for this study can be averaged with other Great Lakes studies to produce regional carbon budgets.

Conclusion

Shoreline erosion can deplete the carbon stock of coastal habitat orders of magnitude faster than the time it took to generate those stocks. This was observed at Illinois Beach State Park where three study sites lost half of the SOC stored within their habitats in the 80 year study period. On decadal timescales, major erosion of carbon occurs during periods of high water level. The high-resolution carbon export data for 2018–2019 showed that major carbon export episodes occur during northeasterly extreme wave events paired with elevated water levels. Low or falling water levels do not lead to increases in the carbon budget, thus these sites are sources of carbon on decadal timescales. While the dominant pattern of the carbon budget at IBSP was loss, the introduction of nourishment sediment appeared to temporarily prevent carbon loss, as seen at site 1 during the record high water levels of the late 1980s. The flux of carbon entering Lake Michigan from these coastal habitats is significant and should be accounted for in regional carbon cycling models. The output of this carbon budget model can assist in the prioritization of conservation efforts by identifying sites with high carbon stocks and carbon accumulation rates.

Resource availability

Lead contact

Further information and requests for resources and materials should be directed to and will be fulfilled by the lead contact, Ethan Theuerkauf (theuerk5@msu.edu).

Materials availability

Direct material requests to lead contact, Ethan Theuerkauf.

Data and code availability

Data presented in this manuscript are publicly available through the Illinois Geospatial Data Clearinghouse under the Coastal category: https://clearinghouse.isgs.illinois.edu/data?field_data_type_value=Coastal. Data presented in this manuscript include "Coastal Habitat Maps along Illinois Beach State Park, derived from aerial and drone imagery, 1939-2020" and "Orthomosaic, digital elevation model, and point cloud derived from unoccupied aerial system (UAS) imagery, Illinois Beach State Park."

METHODS

All methods can be found in the accompanying transparent methods supplemental file.

SUPPLEMENTAL INFORMATION

Supplemental information can be found online at https://doi.org/10.1016/j.isci.2021.102382.

ACKNOWLEDGMENTS

We thank Jenny Bueno, Kevin Engelbert, and Cesar Gutierrez for help with fieldwork and processing of sUAS and sediment samples. Thanks to Brandon Curry for help with preparing samples for radiocarbon dating. We also thank Andrew Masterson for his help at the Northwestern Stable Isotope Laboratory. Habitat delineation data was provided by the Illinois Department of Natural Resources, Illinois Nature Preserves Commission, Illinois Endangered Species Protection Board, and the Natural Heritage Database in August 2018. Funding for this project was provided by the Great Lakes Restoration Initiative through a

grant from the National Oceanic and Atmospheric Administration. This grant was subawarded to the University of Illinois at Urbana-Champaign through Woolpert.

AUTHOR CONTRIBUTIONS

E.T. procured funding, designed the study, conducted hydrodynamic data processing, and supervised all other data processing and analysis. K.B. created habitat maps and conducted carbon analysis. E.T. and K.B. jointly performed field work, updated model, analyzed data, and wrote the manuscript.

DECLARATION OF INTERESTS

The authors declare no competing interests.

Received: December 18, 2020
Revised: March 11, 2021
Accepted: March 28, 2021
Published: May 21, 2021

REFERENCES

Allan, J.D., Smith, S.D.P., McIntyre, P.B., Joseph, C.A., Dickinson, C.E., Marino, A.L., Biel, R.G., Olson, J.C., Doran, P.J., Rutherford, E.S., et al. (2015). Using cultural ecosystem services to inform restoration priorities in the Laurentian Great Lakes. Front. Ecol. Environ. *13*, 418–424, https://doi.org/10.1890/140328.

Angel, J.R. (1995). Large-scale storm damage on the US shores of the Great Lakes. J. Great Lakes Res. *21*, 287–293, https://doi.org/10.1016/S0380-1330(95)71039-5.

As-Salek, J., and Schwab, D.J. (2004). High-frequency water level fluctuations in Lake Michigan. J. Waterw. Port, Coast. Ocean Eng. *130*, 45–53, https://doi.org/10.1061/(ASCE)0733-950X(2004)130.

Atwood, T.B., Connolly, R.M., Almahasheer, H., Carnell, P.E., Duarte, C.M., Lewis, C.J.E., Irigoien, X., Kelleway, J.J., Lavery, P.S., Macreadie, P.I., et al. (2017). Global patterns in mangrove soil carbon stocks and losses. Nat. Clim. Chang. *7*, 523–528, https://doi.org/10.1038/nclimate3326.

Bernal, B., and Mitsch, W.J. (2008). A comparison of soil carbon pools and profiles in wetlands in Costa Rica and Ohio. Ecol. Eng. *34*, 311–323, https://doi.org/10.1016/j.ecoleng.2008.09.005.

Braun, K.N., Theuerkauf, E.J., Hurtgen, M.T., Masterson, A.L., and Horton, D.E. (2020). Loss-on-ignition estimates for soil organic carbon in Great lakes freshwater coastal wetlands. Wetlands *40*, 1201–1206, https://doi.org/10.1007/s13157-020-01270-z.

Braun, K.N., Theuerkauf, E.J., Masterson, A.L., Curry, B.B., and Horton, D.E. (2019). Modeling organic carbon loss from a rapidly eroding freshwater coastal wetland. Sci. Rep. *9*, 1–13, https://doi.org/10.1038/s41598-019-40855-5.

Chrzastowski, M.J., Foyle, A.M., and Trask, C.B. (1996). Erosion and Accretion Trends Along the Lake Michigan Shore at North Point Marina and Illinois Beach State Park. Illinois State Geologial Survey Open File Series. http://hdl.handle.net/2142/45016, 1996–1.

Chrzastowski, M.J., Thompson, T.A., and Brian Trask, C. (1994). Coastal geomorphology and littoral cell divisions along the Illinois-Indiana coast of Lake Michigan. J. Great Lakes Res. *20*, 27–43, https://doi.org/10.1016/S0380-1330(94)71130-8.

Coverdale, T.C., Brisson, C.P., Young, E.W., Yin, S.F., Donnelly, J.P., and Bertness, M.D. (2014). Indirect human impacts reverse centuries of carbon sequestration and salt marsh accretion. PLoS One *9*, 1–7, https://doi.org/10.1371/journal.pone.0093296.

Donato, D.C., Kauffman, J.B., Murdiyarso, D., Kurnianto, S., Stidham, M., and Kanninen, M. (2011). Mangroves among the most carbon-rich forests in the tropics. Nat. Geosci. *4*, 293–297, https://doi.org/10.1038/ngeo1123.

Fritz, Michael, Vonk, Jorien, and Lantuit, Hugues (2017). Collapsing Arctic coastlines. Nature Climate Change *7*, 6–7, https://doi.org/10.1038/nclimate3188.

Ganju, N.K., Defne, Z., Elsey-Quirk, T., and Moriarty, J.M. (2019). Role of tidal wetland Stability in lateral fluxes of particulate organic matter and carbon. J. Geophys. Res. Biogeosci. *124*, 1265–1277, https://doi.org/10.1029/2018JG004920.

Grigoriev, M.N., Rachold, V. 2003. The degradation of coastal permafrost and the organic carbon balance of the Laptev and East Siberian Seas, in: Permafrost: Proceedings of the 8th International Conference on Permafrost, 21-25 July 2003, Zurich, Switzerland. pp. 319–324.

Gronewold, A.D., and Rood, R.B. (2019). Recent water level changes across Earth's largest lake system and implications for future variability. J. Great Lakes Res. *45*, 1–3, https://doi.org/10.1016/j.jglr.2018.10.012.

Hayes, M., Sapkota, Y., White, J., and Cook, R. (2021). Investigating the impact of in situ soil organic matter degradation through porewater spectroscopic analyses on marsh edge erosion. Chemosphere *268*, https://doi.org/10.1016/j.chemosphere.2020.129266.

Hopkinson, C.S., Cai, W.J., and Hu, X. (2012). Carbon sequestration in wetland dominated coastal systems-a global sink of rapidly diminishing magnitude. Curr. Opin. Environ. Sustain. *4*, 186–194, https://doi.org/10.1016/j.cosust.2012.03.005.

Johnston, D.W. (2018). Unoccupied aircraft systems in marine science and conservation. Ann. Rev. Mar. Sci. *11*, 439–463, https://doi.org/10.1146/annurev-marine-010318-095323.

Jorgenson, M.T., and Brown, J. (2005). Classification of the Alaskan Beaufort Sea Coast and estimation of carbon and sediment inputs from coastal erosion. Geo-Marine Lett. *25*, 69–80, https://doi.org/10.1007/s00367-004-0188-8.

Kauffman, J.B., Heider, C., Cole, T.G., Dwire, K.A., and Donato, D.C. (2011). Ecosystem carbon stocks of micronesian mangrove forests. Wetlands *31*, 343–352, https://doi.org/10.1007/s13157-011-0148-9.

Kimball May, S., Dolan, R., and Hayden, B.P. (1983). Erosion of U.S. Shorelines. Eos (Washington. DC) *64*, 521–523.

Lal, R. (2004). Soil carbon sequestration to mitigate climate change. Geoderma *123*, 1–22, https://doi.org/10.1016/j.geoderma.2004.01.032.

Meadows, G.A., Meadows, L.A., Wood, W.L., Hubertz, J.M., and Perlin, M. (1997). The relationship between Great lakes water levels, wave Energies, and shoreline damage. Bull. Am. Meteorol. Soc. *78*, 675–683, https://doi.org/10.1175/1520-0477(1997)078<0675:TRBGLW>2.0.CO;2.

Milne, E., Banwart, S.A., Noellemeyer, E., Abson, D.J., Ballabio, C., Bampa, F., Bationo, A., Batjes, N.H., Bernoux, M., Bhattacharyya, T., et al. (2015). Soil carbon, multiple benefits. Environ. Dev. *13*, 33–38, https://doi.org/10.1016/j.envdev.2014.11.005.

Pendleton, L., Donato, D.C., Murray, B.C., Crooks, S., Jenkins, W.A., Sifleet, S., Craft, C., Fourqurean, J.W., Kauffman, J.B., Marbà, N., et al. (2012). Estimating global "blue carbon" Emissions from conversion and degradation of vegetated coastal ecosystems. PLoS One *7*, https://doi.org/10.1371/journal.pone.0043542.

Sapkota, Y., and White, J.R. (2019). Marsh edge erosion and associated carbon dynamics in coastal Louisiana: a proxy for future wetland-dominated coastlines world-wide. Estuar. Coast. Shelf Sci. *226*, 106289, https://doi.org/10.1016/j.ecss.2019.106289.

Schneider, J., Heaton, D., Leadlay, H., 2007. Extent of Hardened Shoreline, in: State of the Great Lakes 2007. pp. 1–3.

Sapkota, Y., and White, J. (2021). Long-term fate of rapidly eroding carbon stock soil profiles in coastal wetlands. Science of the Total Environment *753*, https://doi.org/10.1016/j.scitotenv.2020.141913.

Smith, P. (2008). Land use change and soil organic carbon dynamics. Nutr. Cycl. Agroecosyst. *81*, 169–178, https://doi.org/10.1007/s10705-007-9138-y.

Spivak, A.C., Sanderman, J., Bowen, J.L., Canuel, E.A., and Hopkinson, C.S. (2019). Global-change controls on soil-carbon accumulation and loss in coastal vegetated ecosystems. Nat. Geosci. *12*, 685–692, https://doi.org/10.1038/s41561-019-0435-2.

Tanski, G., Couture, N., Lantuit, H., Eulenburg, A., and Fritz, M. (2016). Eroding permafrost coasts release low amounts of dissolved organic carbon (DOC) from ground ice into the nearshore zone of the Arctic Ocean. Glob. Biogeochem. Cycles *30*, 1054–1068, https://doi.org/10.1111/1462-2920.13280.

Tanski, G., Wagner, D., Knoblauch, C., Fritz, M., Sachs, T., and Lantuit, H. (2019). Rapid CO 2 release from eroding permafrost in seawater. Geophys. Res. Lett. *46*, 1–17, https://doi.org/10.1029/2019GL084303.

Theuerkauf, E., Braun, K., Kaplan, M., Vivirito, S., Williams, J., and Nelson, D. (2019). Coastal geomorphic response to seasonal lake level rise in the Laurentian Great Lakes, USA. Journal of Great Lakes Research *45* (6), 1055–1068, https://doi.org/10.1016/j.jglr.2019.09.012.

Theuerkauf, E.J., and Rodriguez, A.B. (2017). Placing barrier-island transgression in a blue-carbon context. Earth's Future *5*, 789–810, https://doi.org/10.1002/2017EF000568.

Theuerkauf, E.J., Stephens, J.D., Ridge, J.T., Fodrie, F.J., and Rodriguez, A.B. (2015). Carbon export from fringing saltmarsh shoreline erosion overwhelms carbon storage across a critical width threshold. Estuar. Coast. Shelf Sci. *164*, 367–378, https://doi.org/10.1016/j.ecss.2015.08.001.

Thompson, T.A., and Baedke, S.J. (1997). Strand-plain evidence for late Holocene lake-level variations in Lake Michigan. Bull. Geol. Soc. Am. *109*, 666–682, https://doi.org/10.1130/0016-7606(1997)109<0666:SPEFLH>2.3.CO;2.

Tonelli, M., Fagherazzi, S., and Petti, M. (2010). Modeling wave impact on salt marsh boundaries. Journal of Geophysical Research *115*, 1–17, https://doi.org/10.1029/2009JC006026.

Tranvik, L.J., Downing, J.A., Cotner, J.B., Loiselle, S.A., Striegl, R.G., Ballatore, T.J., Dillon, P., Finlay, K., Fortino, K., Knoll, L.B., et al. (2009). Lakes and reservoirs as regulators of carbon cycling and climate. Limnol. Oceanogr. *54*, 2298–2314, https://doi.org/10.4319/lo.2009.54.6_part_2.2298.

Valentine, K., and Mariotti, G. (2019). Wind-driven water level fluctuations drive marsh edge erosion variability in microtidal coastal bays. Continental Shelf Research *176*, 76–89, https://doi.org/10.1016/j.csr.2019.03.002.

Vonk, J.E., Sanchez-Garca, L., Van Dongen, B.E., Alling, V., Kosmach, D., Charkin, A., Semiletov, I.P., Dudarev, O.V., Shakhova, N., Roos, P., et al. (2012). Activation of old carbon by erosion of coastal and subsea permafrost in Arctic Siberia. Nature *489*, 137–140, https://doi.org/10.1038/nature11392.

iScience, Volume *24*

Supplemental information

The role of short-term and long-term water level and wave variability in coastal carbon budgets

Katherine N. Braun and Ethan J. Theuerkauf

Contents

Figures S1 to S3
Tables S1 to S10
Transparent Methods
Supplemental References

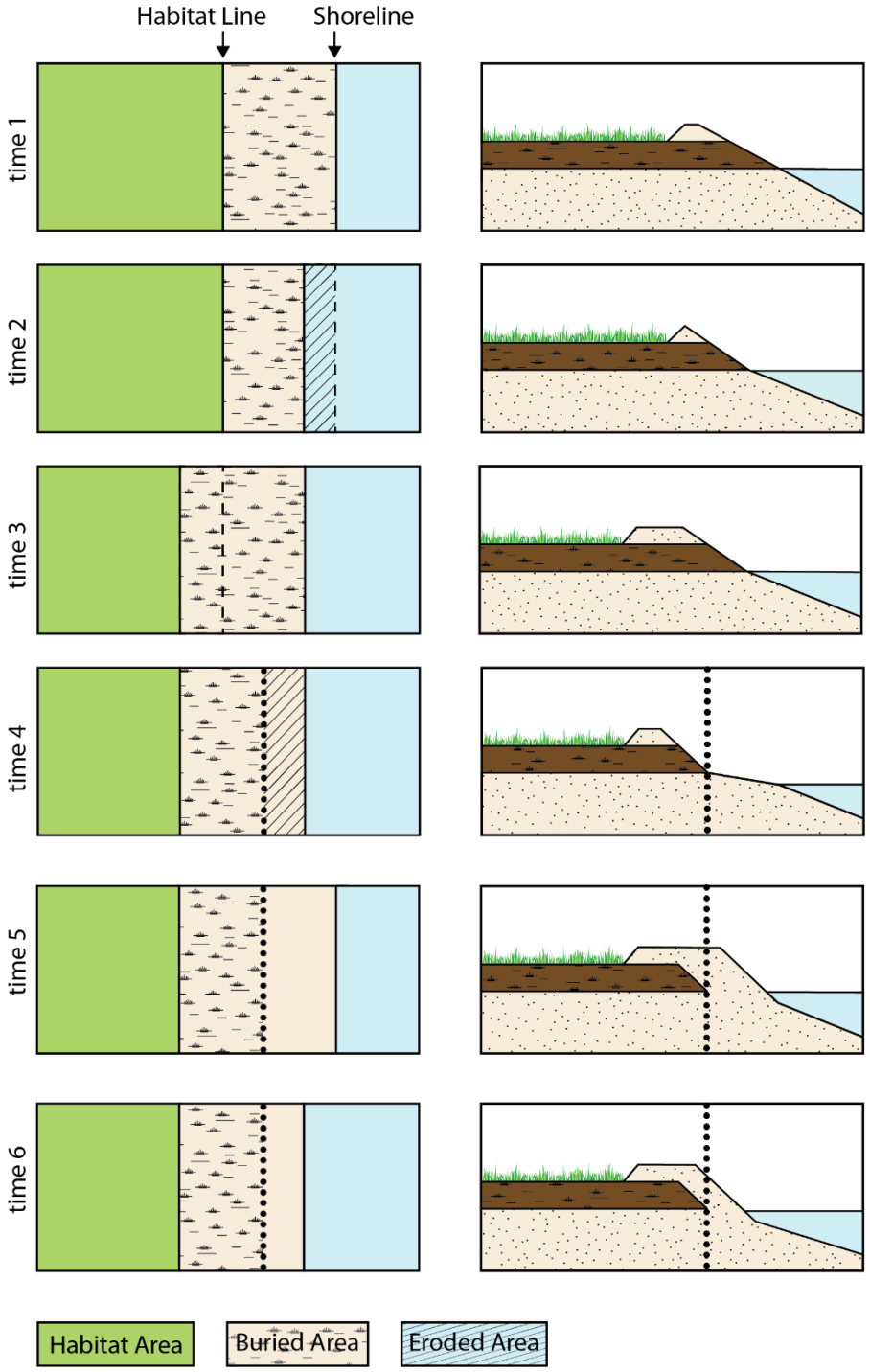

Figure S1. Illustration of habitat change showing habitat area, buried habitat, and eroded habitat. Right column: map view; Left column: cross section. The extent of habitat area is shown in green. Over time, the habitat area shrinks as overwash buries nearshore habitat. The buried habitat is shown in tan overlain with marsh pattern. As habitat is eroded and covered, the extent of buried habitat changes as well. The eroded habitat is denoted with diagonal hash. In the bottom three rows, the dotted line marks the lakeward boundary of the organic unit; lakeward of this line, the organic unit has been completely eroded. Although the beach progrades at time 5, the soil organic unit it not gained back. Therefore the buried habitat area remains landward of the dotted line. Related to Figures 2 and 3.

Braun et al., 2019 Model:

Inputs:

transect area } initial wetland width *1m; overwash width *1m; erosion width *1m

C inventory

Age

Equations	**Units**
$Area_{cell} = A_{initial} + A_{overwash} + A_{erosion}$	m
$CAR = C\ inventory/age$	$gC/m^2/yr$
$Sr = (CAR)(Area_{cell})$	gC/yr
$Er = (Area_{erosion})(C\ inventory)$	gC/yr
$C\ Budget = (Sr - Er)(\Delta t)$	gC
$C\ Stock_{initial} = (C\ inventory)(Area_{cell})$	gC

Updated Model:

Inputs:

area } habitat area; initial buried area; eroded area

C inventory

Age

Equations	**Units**
$Dynamic\ C\ inventory = C\ inventory - (CAR)(t - t_0)$	gC/m^2
$CAR = C\ inventory/age$	$gC/m^2/yr$
$Sr = (CAR)(Area_{habitat})(\Delta t)$	gC
$Er = (Area_{eroded})(Dyn.\ C\ inv.)$	gC
$C\ Budget = Sr - Er$	gC
$C\ Stock_{initial} = (Dyn.\ C\ inv.)(Area_{habitat} + Area_{buried})$	gC

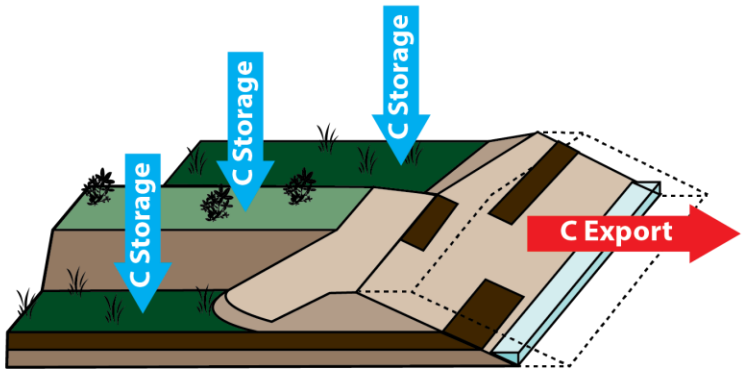

Figure S2. Carbon budget model with updates from previous iteration. Top: original model (Braun et al., 2019) inputs and equations on left, with model updates on right. Changes are denoted with red text. Bottom: Conceptual diagram of the carbon budget box model. Carbon is stored in active habitats and is exported along the erosional shoreface. As the topography and habitat along the shoreline is diverse, the model is split into different spatial cells to account for heterogeneity in carbon content, carbon accumulation rates, elevation of the SOC unit, and erosion. CAR = carbon accumulation rate, Sr = carbon storage, Er = carbon export. Related to Figures 2 and 3.

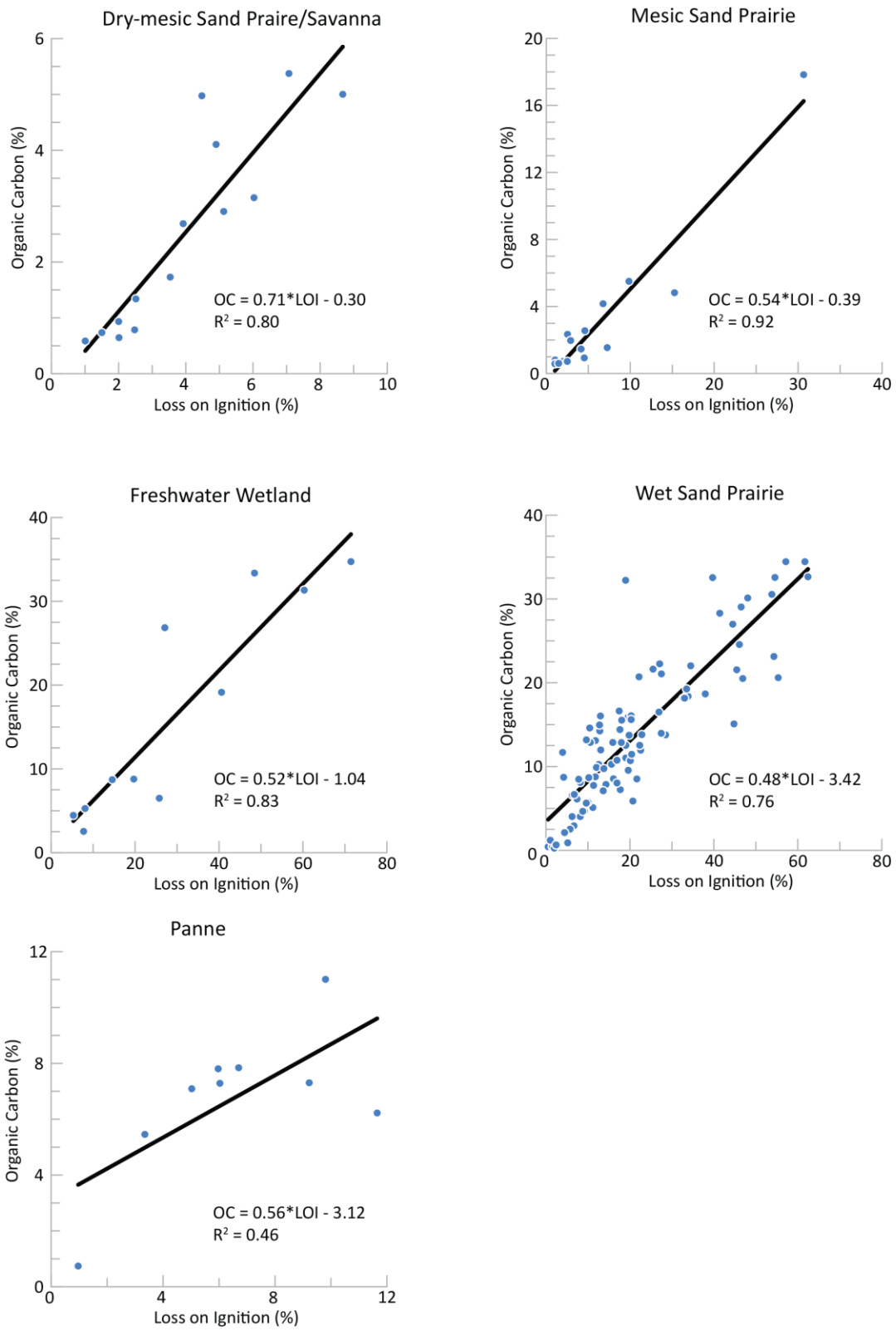

Figure S3. Loss-on-ignition to soil organic carbon regression models for the five carbon-rich habitat types examined in this study. See Braun et al., 2020 for full LOI-SOC modelling methods. Related to Figure 1.

Core #	Northing	Easting	Site	Habitat Type	C Inventory (kgC/m2)	Age (cal yrs BP)	Carbon Accumulation Rate	Carbon-rich Unit Depth (m)
1	645264	343726	1	Wet Sand Prairie	31	1934	16	0.23
2	645215	343620	1	Wet Sand Prairie	81	1934	40	0.5
3	644847	343892	1	Freshwater Marsh	82	830	91	0.5
4	644828	343807	1	Freshwater Marsh	90	830	101	0.67
5	644828	343808	1	Freshwater Marsh	90	830	101	0.57
6	645169	343784	1	Dry-mesic Sand Prairie	5	1934	2	0.12
7	645000	343813	1	Wet Sand Prairie	23	830	26	0.3
8	644985	343841	1	Mesic Sand Prairie	6	830	6	0.22
9	644947	343858	1	Freshwater Marsh	32	830	35	0.5
10	643235	343798	2	Panne	22	394	48	0.46
11	643221	343798	2	Panne	22	394	47	0.41
12	643209	343777	2	Mesic Sand Prairie	12	394	26	0.11
13	643253	343821	2	Panne	17	394	37	0.23
14	642774	343835	3	Mesic Sand Prairie	4	394	9	0.2
15	643607	343768	2	Dry-mesic Sand Prairie	11	394	24	0.3
16	642780	343800	3	Panne	19	394	41	0.3
17	642830	343808	3	Panne	13	394	29	0.25
18	643028	343805	2	Panne	14	394	30	0.25
19	643127	343780	2	Dry-mesic Sand Prairie	7	394	16	0.15
20	643175	343796	2	Dry-mesic Sand Prairie	7	394	16	0.25
21	643310	343777	2	Mesic Sand Prairie	3	394	6	0.2
22	643477	343795	2	Dry-mesic Sand Savanna	3	394	8	0.2
23	643477	343770	2	Dry-mesic Sand Prairie	5	394	11	0.15

Table S1. Sediment core location, habitat type, carbon inventory, age, carbon accumulation rate, and depth of carbonaceous unit. Location data reported in IL East State Plane, meters. Related to Figure 1.

Date	Method
8/1/1939	Aerial
7/15/1946	Aerial
5/1/1961	Aerial
10/6/1974	Aerial
5/1/1993	Aerial
4/1/1997	Aerial
4/22/2000	Aerial
4/20/2002	Aerial
4/5/2004	Aerial
4/7/2005	Aerial
4/16/2006	Aerial
4/26/2007	Aerial
7/31/2008	Aerial
5/16/2009	Aerial
4/13/2010	Aerial
4/11/2012	Aerial
4/22/2014	Aerial
3/27/2017	Aerial
7/24/2018	UAS
8/31/2018	UAS
9/11/2018	UAS
10/8/2018	UAS
10/24/2018	UAS
11/5/2018	UAS
12/18/2018	UAS
1/18/2019	UAS
3/28/2019	UAS
4/25/2019	UAS
6/6/2019	UAS
6/17/2019	UAS
7/10/2019	UAS
7/26/2019	UAS

Table S2. Dates of acquired imagery, with method. Aerial: historic aerial imagery sourced from the Lake County, Illinois Planning, Building, and Development Department. UAS: unoccupied aerial system, aka, drone. Related to Figures 2 and 3.

Sample Name: Depth (cm)	Lab Code (UCIAMS#)	Northing	Easting	RCYBP	2 Sigma Range (cal yrs BP)	2 Sigma Average (cal yrs BP)
RC1: 50-51	219580	644829.8	343870.2	920 ± 60	725-935	830 ± 60
RC4: 28-29	219583	642878.4	343806.1	300 ± 20	353-435	394 ± 20
C3: 36.5-37.5	196986	645164.9	343612.4	2105 ± 20	2004-2136	2070 ± 20
C4: 24-25	196987	645372	343633.2	1860 ± 20	1729-1865	1797 ± 20

Table S3. Radiocarbon dates and sample number for the University of California Irvine AMS facility. Dates are presented in uncalibrated and calibrated years (using CALIB 7.1 and IntCal 13). Ages used for the carbon budget model are the average of the two sigma age range provided by CALIB. Location data reported in IL East State Plane, meters. Related to Figure 1.

Habitat Type	# of Cores	Avg Core Depth	Carbon Inventory	Carbon Accumulation Rate
		m ± σ	$gC/m^2 \pm \sigma$	$gC/m^2/yr \pm \sigma$
Dry Mesic Sand Prairie/Savanna	6	0.20 ± 0.07	6545 ±2744	13 ± 8
Mesic Sand Prairie	4	0.18 ± 0.05	6179 ± 3984	12 ±9
Panne	6	0.32 ± 0.10	17757 ± 3735	38 ± 8
Wet Sand Prairie	3	0.34 ± 0.14	45163 ± 30932	27 ± 13
Freshwater Marsh	4	0.56 ± 0.08	73565 ± 28175	82 ± 31
Foredune	n/a	n/a	0	0

Table S4: Average values for the core depth, carbon inventory, and carbon accumulation rate for each habitat type, Related to Figures 1 and 6.

Date	DMSPS	Foredune	Freshwater Marsh	Mesic Sand Prairie	Wet Sand Prairie	Total
8/1/1939	98940	0	45537	37553	19954	201984
7/15/1946	87398	0	41280	38344	19954	186976
5/1/1961	76587	0	36199	27937	19954	160677
10/6/1974	37982	8418	16935	23719	19954	107008
5/1/1993	37507	11299	16935	24799	19954	110494
4/1/1997	36318	17881	16935	24784	19954	115871
4/22/2000	39198	19348	16935	24934	19954	120369
4/20/2002	38878	19480	16935	24934	19954	120180
4/5/2004	38622	19394	16935	24920	19954	119824
4/7/2005	37636	20028	16935	24867	19954	119419
4/16/2006	36486	19265	16935	24753	19954	117392
4/26/2007	35946	18321	16935	24728	19954	115884
7/31/2008	36048	18142	16935	24727	19954	115805
5/16/2009	35975	17689	16935	24727	19954	115278
4/13/2010	35854	17403	16935	24727	19954	114872
4/11/2012	32925	16744	16935	24381	19954	110938
4/22/2014	31472	15175	16935	24157	19954	107693
3/27/2017	22630	9659	16935	22467	19167	90858
7/24/2018	19295	9215	16935	21301	17511	84257
8/31/2018	19274	9181	16935	21245	17525	84160
9/11/2018	19172	9119	16935	21151	17443	83819
10/8/2018	19167	9055	16935	21128	17428	83714
10/24/2018	19140	8999	16935	21092	17404	83571
11/5/2018	19060	8925	16935	20937	17257	83114
12/18/2018	18672	8735	16926	20394	17037	81765
1/18/2019	18633	8652	16925	20109	17016	81335
3/28/2019	18579	8539	16916	20099	16992	81126
4/25/2019	18333	8436	16908	19916	16726	80318
6/17/2019	18564	8688	16893	20627	16724	81496
7/10/2019	18574	8680	16893	20643	16723	81512
7/26/2019	18579	8669	16889	20636	16759	81531

Table S5: Habitat extent (m^2) for Site 1. DMSPS = dry-mesic sand prairie/savanna. Related to Figure 6.

Date	DMSPS	Mesic Sand Prairie	Panne	Total
8/1/1939	178275	43758	6378	228411
7/15/1946	174535	44072	6378	224984
5/1/1961	160293	41574	6378	208245
10/6/1974	143499	38796	6378	188672
5/1/1993	99421	26138	6378	131937
4/1/1997	97173	24980	6378	128531
4/22/2000	93037	22521	6378	121937
4/20/2002	91143	22914	6378	120435
4/5/2004	94012	24802	6378	125192
4/7/2005	92910	23559	6378	122847
4/16/2006	92290	24097	6378	122765
4/26/2007	91261	23477	6378	121116
7/31/2008	92116	24037	6378	122531
5/16/2009	90600	23966	6378	120945
4/13/2010	88152	23952	6378	118482
4/11/2012	81333	21420	6378	109131
4/22/2014	83066	21708	6378	111152
3/27/2017	61013	17331	4709	83053
7/24/2018	49226	15066	1950	66242
8/31/2018	48827	15058	1955	65840
9/11/2018	48199	14980	1904	65083
10/8/2018	48135	14972	1904	65011
10/24/2018	48007	14968	1858	64833
11/5/2018	47618	14892	1826	64336
12/18/2018	46280	14661	1466	62407
1/18/2019	46235	14644	1375	62254
3/28/2019	46154	14522	1289	61966
4/25/2019	44775	14237	1071	60084
6/17/2019	44075	14238	1094	59407
7/10/2019	43677	14203	1091	58970
7/26/2019	43660	14204	1087	58951

Table S6: Habitat extent (m^2) for Site 2. DMSPS = dry-mesic sand prairie/savanna. Related to Figure 6.

Date	Foredune	Mesic Sand Prairie	Panne	Total
8/1/1939	18948	86507	24122	129577
7/15/1946	21671	77965	24268	123905
5/1/1961	8656	65926	24055	98638
10/6/1974	6827	79701	27345	113873
5/1/1993	1000	66500	20260	87760
4/1/1997	868	65592	20027	86487
4/22/2000	869	66520	20417	87806
4/20/2002	2129	69305	21953	93388
4/5/2004	2055	65820	21549	89425
4/7/2005	2102	66494	21915	90511
4/16/2006	2102	65619	21925	89646
4/26/2007	2103	64313	22004	88421
7/31/2008	2103	64395	22429	88926
5/16/2009	2572	64694	22722	89988
4/13/2010	2571	64206	22712	89488
4/11/2012	2404	62686	22609	87699
4/22/2014	2405	61704	22062	86171
3/27/2017	1685	51732	17774	71191
7/24/2018	739	48319	13280	62339
8/31/2018	736	48341	13275	62352
9/11/2018	730	48278	12968	61976
10/8/2018	730	48233	12872	61835
10/24/2018	730	48147	12858	61734
11/5/2018	709	48113	12675	61496
12/18/2018	702	47207	11697	59606
1/18/2019	670	47023	11564	59257
3/28/2019	661	46920	11452	59033
4/25/2019	648	46580	10995	58224
6/17/2019	678	46537	11089	58304
7/10/2019	651	46448	11146	58246
7/26/2019	651	46457	11296	58405

Table S7: Habitat extent (m^2) for Site 3. Related to Figure 6.

Date	DMSPS	Freshwater Marsh	Mesic Sand Prairie	Wet Sand Prairie
8/1/1939				
7/15/1946	9744	4833	1778	0
5/1/1961	11486	7206	11083	0
10/6/1974	30478	11602	6398	0
5/1/1993	683	0	0	0
4/1/1997	322	0	0	0
4/22/2000	43	0	0	0
4/20/2002	288	0	0	0
4/5/2004	1945	0	0	0
4/7/2005	130	0	0	0
4/16/2006	701	0	0	0
4/26/2007	8	0	0	0
7/31/2008	196	0	86	0
5/16/2009	0	0	0	0
4/13/2010	692	0	0	0
4/11/2012	2131	0	122	0
4/22/2014	3064	0	267	0
3/27/2017	7433	0	624	402
7/24/2018	6574	0	1579	983
8/31/2018	24	0	53	13
9/11/2018	97	0	75	120
10/8/2018	134	0	63	46
10/24/2018	30	0	0	2
11/5/2018	35	0	14	3
12/18/2018	29	0	0	0
1/18/2019	15	0	0	20
3/28/2019	4	0	0	0
4/25/2019	22	0	27	114
6/17/2019	204	0	299	310
7/10/2019	24	0	154	101
7/26/2019	4	0	5	0

Table S8: Eroded habitat area (m^2) for Site 1. DMSPS = dry-mesic sand prairie/savanna. Date refers to second survey date, e.g., 7/15/1946 row contains area eroded between 8/1/1939 and 7/15/1946. Related to Figure 6.

Date	DMSPS	Mesic Sand Prairie	Panne
8/1/1939			
7/15/1946	18450	4606	0
5/1/1961	13838	1213	0
10/6/1974	14979	2437	0
5/1/1993	29124	10028	0
4/1/1997	10916	2731	0
4/22/2000	5404	29	0
4/20/2002	4013	160	0
4/5/2004	2135	1374	0
4/7/2005	3965	722	0
4/16/2006	1218	98	0
4/26/2007	418	56	0
7/31/2008	759	264	0
5/16/2009	491	0	0
4/13/2010	2773	563	0
4/11/2012	3164	871	0
4/22/2014	14	0	0
3/27/2017	26070	6225	1143
7/24/2018	38013	7688	2425
8/31/2018	494	83	137
9/11/2018	463	17	106
10/8/2018	378	37	438
10/24/2018	127	0	198
11/5/2018	214	11	1
12/18/2018	525	78	15
1/18/2019	143	0	90
3/28/2019	208	100	0
4/25/2019	1037	200	0
6/17/2019	1393	79	468
7/10/2019	331	0	120
7/26/2019	615	186	1

Table S9: Eroded habitat area (m^2) for Site 2. DMSPS = dry-mesic sand prairie/savanna. Date refers to second survey date, e.g., 7/15/1946 row contains area eroded between 8/1/1939 and 7/15/1946. Related to Figure 6.

Date	Mesic Sand Prairie	Panne
8/1/1939		
7/15/1946	1150	49
5/1/1961	2620	959
10/6/1974	6577	7075
5/1/1993	8472	6706
4/1/1997	147	0
4/22/2000	614	0
4/20/2002	3268	0
4/5/2004	146	0
4/7/2005	922	0
4/16/2006	574	0
4/26/2007	2160	0
7/31/2008	1096	0
5/16/2009	0	0
4/13/2010	40	0
4/11/2012	2427	0
4/22/2014	929	295
3/27/2017	8307	1637
7/24/2018	5030	2981
8/31/2018	314	57
9/11/2018	63	457
10/8/2018	137	319
10/24/2018	32	74
11/5/2018	384	0
12/18/2018	384	4
1/18/2019	10	60
3/28/2019	0	3
4/25/2019	256	4
6/17/2019	394	175
7/10/2019	185	143
7/26/2019	240	187

Table S10: Eroded habitat area (m^2) for Site 3. Date refers to second survey date, e.g., 7/15/1946 row contains area eroded between 8/1/1939 and 7/15/1946. Related to Figure 6.

Transparent Methods

Study Site

We created a SOC budget at three coastal sites at Illinois Beach State Park (IBSP). IBSP is a 4,160-acre park situated on the Zion Beach Ridge Plain along the shore of Lake Michigan in northeastern Illinois, USA (42.468943, -87.806605; Figure 1). Radiocarbon dating and stratigraphic mapping of the area has shown that this beach ridge plain first appeared along the Illinois coastline around 3,700 years BP (Larsen, 1985). Along the IBSP shoreline, some stretches are natural and lack anthropogenic modification while others have been hardened over the past century. Concrete cube revetments, sheet pile groins, and rip rap retaining walls exist in various places along the shoreline and have exacerbated erosion at various points over the past several decades when the downdrift shoreline moves landward of this shoreline protection (Theuerkauf et al., 2019). The sites examined in this study are all located within the erosional northern portion of the park.

Site 1 is immediately downdrift from a hardened shoreline (Figure 1). The northern portion of Site 1 has little beach; habitat extends directly to the erosive shoreline except in areas with washover fans. The southern portion of the site has a sandy beach and low elevation (<1.5 m) foredunes. Site 2 is immediately south of a hardened shoreline. Similar to the northern portion of Site 1, habitat at Site 2 extends directly to the erosive shoreline except at two panne wetland depressions which were actively being filled with washover deposits during the study period. Site 3 is immediately south of Site 2. The northern third of Site 3 is a broad washover terrace that is filling in low elevation panne wetlands. The middle of Site 3 contains an ephemeral beach fronting a 1-2 m scarp formed from an eroding beach ridge. The southern portion of the site contains another washover terrace with a small section of short (<1 m) foredune.

Six habitat types were monitored at these study sites. These habitat delineations and plant species data were sourced from the Illinois Natural Areas Inventory. Mesic sand prairie is a native grassland community that experiences fluctuating water table elevation, with dominant species including

Schizachyrium scoparium (little bluestem), *Andropogon gerardii* (big bluestem), and *Sorghastrum nutans* (Indian grass). Dry-mesic sand prairie/savanna is the combination of two habitat types (dry-mesic sand prairie and dry-mesic sand savanna) which are difficult to distinguish over decadal timescales due to the fluid boundary between prairie and savanna. The carbon inventories as well as the soil characteristics acquired from sediment cores taken in the dry-mesic sand prairie and dry-mesic sand savanna were similar, providing further justification to combine these habitats into one for the purposes of the carbon budget model. Dominant species in this habitat include *Sorghastrum nutans* (Indian grass), *Schizachyrium scoparium* (little bluestem), and *Quercus velutina* (black oak). Panne habitats are groundwater fed wetlands that occupy swales, with dominant species including *Calamagrostis canadensis* (blue-joint grass) and *Cladium mariscoides* (twig-rush). Wet sand prairie is a tall grassland community with sandy, wet soils; dominant species include *Calamagrostis canadensis* (blue-joint grass), *Spartina pectinata* (prairie cordgrass), and *Carex bicknellii* (Bicknell's sedge). Freshwater marsh habitat is distinguished from the wet sand prairie due to the prolonged periods of inundation. Dominant species include S*cirpus validus* (great bulrush) and *Typha angustifolia* (narrow-leaf cattail). Finally, foredune is a sandy dune community dominated by *Arctostaphylos uva-ursi* (bearberry), *Juniperus horizontalis* (trailing juniper), and *Ammophila breviligulata* (beach grass). Foredune habitat is not included as an input in the carbon budget model as field surveys and coring revealed that this habitat has no organic soil unit.

The dominant Lake Michigan water level patterns that facilitate geomorphic change on management-relevant timescales occur over storm event, seasonal, annual, and decadal timescales. Superimposed on these shorter timescale oscillations are longer-term variations, such as 150 year and 500 year cycles, that can exacerbate the shorter-term fluctuations (Thompson, 1992; Thompson and Baedke, 1997). Over the past century, Lake Michigan water levels have fluctuated between above average and below average levels approximately every decade with record high water levels occurring in the mid-1980s and in 2020 and record low water levels occurring in the mid-2000s; the long-term average water level is 176.606 m NAVD88 (Figure 2). Annual and seasonal cycles of water level variability occur on

top of these decadal cycles and erosion along Great Lakes shorelines occurs in temporally dynamic periods related to these water level cycles (Angel, 1995; Meadows et al., 1997; Theuerkauf et al., 2019). Peak annual water levels typically occur during the late summer and minimum water levels typically occur during the winter, however, there are year-to-year variations in the timing and magnitude of the highs and lows (Quinn, 2002). In 2014, Lake Michigan water levels rapidly increased from record low levels in 2013 to above average levels (Gronewold et al., 2016). Water levels have been rising ever since and are now (2020) at record highs. Periods of high water level allow waves to reach further up the beach profile and generate shoreline erosion and SOC export (Braun et al., 2019; Meadows et al., 1997; Theuerkauf et al., 2019).

Carbon Content and Radiocarbon Age Dating: Generation of Carbon Inventories and Accumulation Rates

Soil organic carbon was measured from sediment core samples collected from five habitat types at the three study sites. Twenty-three sediment cores were collected using a backpack-mounted vibracore system. Cores were taken to the point of refusal, which was generally a sand layer underlying the organic sediments, and compaction was recorded. The cores were split, photographed, described, and the organic sediments were sampled every 5 cm downcore. Samples were dried in a 100°C oven, then combusted in a muffle furnace to measure loss-on-ignition (LOI; see Braun et al., 2020 for processing details). Elemental analysis was conducted on a subset of 48 samples at the Northwestern University Isotope Ratio Mass Spectrometry facility to create LOI to SOC models for each habitat type (Braun et al., 2020; Craft et al., 1991). The LOI-SOC models used in this study are reported in Figure S3. These habitat-specific LOI to SOC models were used to convert the LOI results to SOC for all samples. The carbon inventory of each core was calculated by summing the carbon contained within each sample in that core (Table S1; Table S4).

Radiocarbon age dates were generated to determine the rate of carbon accumulation. Aboveground biomass material (e.g., leaves and seeds) were hand-picked from the base of the organic

sediments, washed, examined under a dissecting microscope to ensure no submerged aquatic materials were chosen, and stored in 18% HCl. Samples were sent to the University of California-Irvine for radiocarbon dating in the Walter M Keck Carbon Cycle Accelerator Mass Spectrometer. Ages were calibrated using Calib 7.1 and IntCal 13 (Reimer et al., 2013; Table S3). With these samples, we make the assumption that this material was deposited very close in time to when the organic-rich sediments formed, thus the age date can be used to derive the age of the habitat (Braun et al., 2019; Redfield and Rubin, 1962; Theuerkauf et al., 2015). Using this assumption, we generate the carbon accumulation rate through division of the carbon inventory by the age of that organic unit relative to the time of sample collection, i.e., 2018 AD (Table S1). We used a single age date, the average of the two-sigma calibration, in the carbon budget model; the range of radiocarbon dates possible for these samples were included in the error analysis and is therefore represented by the shaded areas in the model results (Figures 2, 3, and 5). At Site 1, the northern radiocarbon date, 1934 cal yrs BP, is the average of two dates taken in close proximity (140 m) to each other: 2070 and 1797 cal yrs BP.

Habitat-specific carbon inventories and carbon accumulation rates are used in our SOC budget model to account for spatial heterogeneity in SOC across different habitats at a given study site (Table S4; Figure 1). These habitat-specific values were created based on the average value of the carbon inventory collected in a specific habitat type across all three sites. Generating habitat-specific SOC data, rather than assuming that SOC is uniform across a study site, allows for a more accurate characterization of the actual carbon storage at a site and allows the SOC data generated in this study to be generalized to other similar coastal habitats throughout the region.

Habitat Area Delineation

The boundaries between different habitat types were provided as shapefiles by the Illinois Natural Areas Inventory (INAI). The Inventory provides data on high quality natural areas in the state, including extent, habitat quality, and species presence at time of survey. The habitat boundaries for the three sites were based on the most recent INAI surveys of the sites, which were conducted in 1976. Habitat areas for

each time period examined in this study were generated by comparing the habitat boundary shapefiles to both historic aerial photography as well as modern aerial photography generated with a small-unoccupied aerial system (sUAS). Historic georeferenced aerial photography were acquired for the period 1939-2017 from the Lake County, Illinois Planning, Building, and Development Department. These are decadal imagery with the exception of approximately annual imagery from 2000 to 2017 (Table S2). sUAS, commonly known as drones, were used to acquire monthly orthomosaic images and digital elevation models of the three study sites from July 24, 2018 to July 26, 2019. Habitat area extents are presented in Tables S5-7.

For the purposes of this study we define the habitat area as the extent of habitat that is actively storing carbon, i.e., habitat that has not been covered by washover or beach sediment. Two sets of base habitat area shapefiles were created, one for the long-term record (1939-2017) and one for the short-term record (July 24, 2018-July 26, 2019). The INAI shape files were compared to both the historic aerial photographs and the 2018-2019 imagery to corroborate that the habitat boundaries were valid for the time period represented in the image. Boundaries that were no longer accurate (i.e., land use changes that altered habitat types; e.g., subdivision to prairie) were modified using ESRI ArcGIS 10.5.1 to align with the aerial imagery. The habitat areas of the northern portion of Site 1 were hand digitized following aerial images as the INAI did not cover the entire site.

The validated northern, western, and southern boundaries of the habitat areas remained static through time with only the eastern boundary changing as shoreline erosion and overwash impacted the lakeward edge of the habitat areas. The habitat line is the boundary between actively growing habitat and the beach or washover fan. This habitat line was digitized based on the historic aerial photographs and sUAS orthomosaic images of the three study sites. Habitat was included on washover fans or beaches if vegetation had colonized >75% of the bare earth. The initial habitat line was digitized using ESRI ArcGIS 10.5.1 for the 1939 aerial photographs, then each subsequent photograph or othomosaic's habitat line was digitized using the previous time-step's habitat line as a base to reduce digitization error (i.e., only true

change was digitized). The shoreline, defined as the wet/dry line, was digitized from the photographs and orthomosaics as well. For the modern sUAS record, the erosion line, defined as the elevation contour of the base of the organic soil unit, was generated from the digital elevation models.

In addition to the active habitat areas, the buried and eroded habitat areas were digitized (Figure S1). We define a buried habitat area as an area where a unit of organic sediments is overlain by beach or washover sediment. Buried areas occur on the shoreline where overwash has covered previously productive habitat. While the habitat is no longer storing additional carbon as the vegetation has been buried, the organic sediments are undisturbed and carbon remains stored. We define an eroded habitat area as the extent of land with organic sediments that has been eroded. Both the buried and eroded habitat areas were digitized from digital elevation models that were generated from the sUAS surveys.

The areal extent of buried and eroded areas is determined based on the spatial relationships between the habitat line, shoreline, and erosion lines (Figure S1). In contrast to the previous SOC budget modeling study, we did not assume that the soil organic unit extended under the entire shoreface to the shoreline for the modern, sUAS record. Instead, we used elevation data from the DEMs and the depth of the organic units from sediment cores to determine the eastern boundary of the soil organic unit.

Details on Mapping of Eroded and Buried Habitat Areas

For the modern sUAS record, the erosion line, defined as the elevation contour of the base of the organic soil unit, was generated from the digital elevation models. Compaction was added to the depth of the organic units from the cores to accurately determine the elevation of the organic unit base. We assumed that compaction was evenly distributed among the whole core, thus a portion of the total compaction was added to each lithologic unit. The topographic contour of this calculated elevation of the base of the organic unit was extracted from the DEM. If that elevation contour was positioned landward of the shoreline, the contour was used as the erosion line for determining the buried areas and eroded areas at that time-step (i.e. shoreline erosion has yet to reach buried organic unit). If the erosion contour was at or lakeward of the shoreline, then the shoreline was used in place of the erosion line at that time-

step (i.e. shoreline erosion has already begun excavating the buried organic unit). This method of using the elevation of the base of the organic unit does not account for partial erosion of the soil profile; erosion is only measured when the full soil profile has been excavated by coastal erosion. For the historic record (1939-2017), no such elevation data exists, therefore the buried area was assumed to extend to the shoreline.

The buried area is the area between the habitat line and the shoreline or erosion line. Sand could be redistributed across the shoreface after an erosional event and cause the erosion line to be further lakeward than the previous time-step. Using this erosion line would inaccurately extend the buried area lakeward where the soil organic unit had already been eroded. To avoid this issue, the lakeward boundary of each buried area did not extend lakeward past previous contour lines (see Figure S1, time 5 for an illustration of this scenario).

The eroded area is the area of the soil organic unit that was eroded between two time-steps (Tables S8-10). The eroded area is either between two shorelines, a shoreline and an erosion line, or two erosion lines. Similar to the buried area, if the erosion line or shoreline extended landward at a previous time-step, then the eroded areas in all time-steps after that period only include erosion that extends landward beyond the initial line. This ensures that the eroded area does not double count erosion by including the erosion of non-carbonaceous sand. Erosion lines were only produced for the short-term sUAS record as topographic data does not exist for the historic aerial photographs. In these images it was assumed that the soil organic unit extended to the shoreline and the buried areas and eroded areas were digitized accordingly.

The error associated with digitization of the habitat, buried, and eroded areas was calculated for inclusion in the carbon budget model error. The difference between the sum of the eroded areas for each time bin during the study and the difference between the initial and final habitat and buried areas should be zero. The average difference was 51 m^2, which is considered the error for the digitization technique.

The historic aerial imagery revealed that significant habitat change occurred between 1939 and 1974. The habitat area boundaries at these three sites were modified based on the historic aerial imagery

to reflect these changes. At Site 1, the dry-mesic sand prairie/savanna that extended along the southern portion of the site became exposed to the shoreline through erosion and converted to foredune habitat, as seen in the 1974 aerial images. At Site 3, a subdivision development visible in the early historic photographs was demolished and the area converted to prairie between 1946 and 1974; this event accounts for the decline and subsequent rebound in habitat area during this period.

sUAS Methods

A DJI Phantom 4 Pro quadcopter small unoccupied aerial system was used to collect topography data at each study site. The sUAS has a 1-inch, 20 megapixel RGB sensor on a gimbal mounted camera. Predetermined flights were created using the DJI Ground Station Pro application to ensure consistency between surveys. The sUAS was flown nadir at an altitude of 70-80 m depending on the site, capturing JPEG files with resolutions of 0.021 m per pixel. Images were captured with 90% front overlap and 80% side overlap. The geographic positions of the cameras were calculated using the onboard GPS/GLONASS satellite positioning systems. Ten to fifteen black and white checkered baseball plates were used as ground control points and placed throughout the study area. The ground control points were evenly distributed to account for varying topography along the extent of the sites. These points were surveyed using a Trimble Geo7X Centimeter Edition NRTK-GPS system with ~0.02 m horizontal and vertical errors. sUAS data were only collected during calm wave conditions (waves <0.5 m) to ensure maximum beach areal coverage. Structure-from-motion photogrammetry, conducted with Agisoft Metashape Professional software, was used to generate orthomosaic images and DEMs from the aerial photography and GPS survey data (Goncalves and Henriques, 2015; Turner et al., 2016).

Hydrodynamic Data

Lake Michigan water level data were downloaded from the NOAA Tides and Currents webpage for the Calumet Harbor (Chicago) water level gauge (ID: 9087044). Daily data were downloaded for January 1, 1939 to August 1, 2019, and hourly water level data were downloaded for July 24, 2018 to July 26, 2019 to correspond with the sUAS data record. Wave data, including significant wave height and

wave direction, for the Waukegan, IL Buoy (Station ID: 45186) were downloaded from the NOAA National Data Buoy Center. Hourly data were downloaded for July 24, 2018 to November 29, 2018 and April 18, 2019 through July 26, 2019. Model data (significant wave height and wave direction) were provided by the NOAA Great Lakes Environmental Research Lab to fill in the data gaps arising from winter buoy removal. The model data was generated from the Nowcast of the Great Lakes Coastal Forecasting System (Chu et al., 2011; NOAA GLERL, 2019). Only onshore (0 to 180°) waves were included in the analysis. The extreme wave threshold, defined as the highest 2% of all wave heights, was calculated for the entire dataset, and then the percentage of extreme waves in each time-step was calculated. Wave rose diagrams for the extreme waves were created for time-steps with high-magnitude storm events (Figure 4; August 31, 2018 to September 11, 2018; October 24, 2018 to November 5, 2018; November 5, 2018 to December 18, 2018; March 28, 2019 to April 25, 2019).

Carbon Budget Model

We updated the carbon budget from Braun et al., (2019) to include more spatially and temporally dynamic terms. Both budgets take a simple mass-balance approach by comparing the amount of carbon stored across a habitat area with the amount of carbon lost through shoreline erosion (Figure S2). The budget is parameterized with three inputs: carbon inventory, habitat age, and geospatial data on habitat change (topographic and areal extent change).

The carbon accumulation rate is calculated by dividing the carbon inventory of a habitat by the age of that habitat. The carbon storage term is very similar to the term in the original model: carbon storage is the product of the carbon accumulation rate, the area of active habitat, and the time-step. Unlike in the original model, the carbon storage and carbon export terms are not expressed as rates, but rather as amounts of carbon to facilitate ease of interpretation; rates of carbon storage and export normalized by area are also presented in the results. Carbon storage is presented as the product of the carbon accumulation rate, the habitat area, and the time-step length. Carbon export is the product of the area eroded and the dynamic carbon inventory. The net carbon, or carbon budget, is simply the difference

between carbon storage and carbon export. The carbon stock is calculated for the initial time-step, 1939, as the product of the dynamic carbon inventory and the sum of the habitat area and the buried area. This ensures that any carbon contained underneath a washover fan or buried under the beach is incorporated into the carbon stock. The stock for each time-step after the initial one is the sum of the previous carbon stock and the net carbon for that time-step. Instead of using multiple model "cells" across a 1 m wide shore-normal transect, we implemented a spatially comprehensive modification to the Braun et al., (2019) model. Each site was split into habitat types and a separate carbon budget was calculated for each habitat based on the average carbon inventory and age of that habitat's organic sediments. The carbon budget for the entire site is generated by summing up the budgets for each of the individual habitats.

In this study, we updated the carbon export term to better reflect ravinement of the organic sediments due to shoreface erosion. Carbon export is the product of the area of land eroded and the dynamic carbon inventory. In the first version of this model, the area of erosion was measured using shoreline position (Braun et al., 2019). However, wave action impinging on the upper shoreface can erode the soil organic unit without contemporaneous landward migration of the shoreline. To address this, we used topography data from the drone DEMs to extract the elevation contour that corresponded to the base of the organic soil unit. Using the elevation of the base of the organic soil unit as the metric for soil carbon erosion ensures that only removal of the entire soil organic carbon unit is included in the model.

The model uses a carbon inventory to calculate the carbon stocks of the organic sediments. Soil carbon stocks are frequently parameterized using carbon content and dry bulk density data (i.e., Lee et al., 2009; Walter et al., 2016). However, compaction due to coring methods has been shown to overestimate SOC stocks due to the reduction in the thickness of the soil profile (Smeaton et al., 2020). The carbon inventory, which is the total amount of SOC per unit area, is not impacted by compaction as it sums the amount of carbon contained in the entire organic unit, and thus is a robust measure of the total amount of organic carbon contained within the carbonaceous units.

In order to properly characterize decadal SOC dynamics we updated the method for calculating the carbon inventory through time. When deriving carbon budgets on decadal timescales, the carbon inventory should increase through time based on the carbon accumulation rate (CAR; static carbon inventory/age). Therefore, the carbon inventory for all time periods before 2018-2019 (the period during which the carbon inventory was measured, as the carbon content and radiocarbon dating were carried out on samples collected during this time), was parameterized as the dynamic carbon inventory:

$$\text{Dynamic C Inventory for } t = \text{C Inventory} - (\text{CAR}*(t - t_o))$$

We examined carbon dynamics on two scales: a long-term, decadal scale with the full carbon budget, and a short-term, high resolution scale using monthly drone data. As the carbon budget relies on inputs that use average carbon dynamic values, we did not calculate carbon storage for the short-term record. Using a carbon accumulation rate that does not take into account the seasonal dynamics in these temperate habitats would not produce an accurate budget for monthly time-steps. Instead, we calculated the export of carbon during the short term record to examine the coastal processes causing carbon loss.

Supplemental References

Angel, J.R., 1995. Large-scale storm damage on the US shores of the Great Lakes. J. Great Lakes Res. 21, 287–293. https://doi.org/10.1016/S0380-1330(95)71039-5

Braun, K.N., Theuerkauf, E.J., Hurtgen, M.T., Masterson, A.L., Horton, D.E., 2020. Loss-On-Ignition Estimates for Soil Organic Carbon in Great Lakes Freshwater Coastal Wetlands. Wetlands. 40, 1201-1206. https://doi.org/10.1007/s13157-020-01270-z

Braun, K.N., Theuerkauf, E.J., Masterson, A.L., Curry, B.B., Horton, D.E., 2019. Modeling organic carbon loss from a rapidly eroding freshwater coastal wetland. Sci. Rep. 9, 1–13. https://doi.org/10.1038/s41598-019-40855-5

Chu, P.Y., Kelley, J.G.W., Mott, G. V., Zhang, A., Lang, G.A., 2011. Development, implementation, and skill assessment of the NOAA/NOS Great Lakes Operational Forecast System. Ocean Dyn. 61, 1305–1316. https://doi.org/10.1007/s10236-011-0424-5

Craft, C.B., Seneca, E.D., Broome, S.W., 1991. Loss on Ignition and Kjeldahl Digestion for Estimating Organic Carbon and Total Nitrogen in Estuarine Marsh Soils: Calibration with Dry Combustion. Estuaries 14, 175. https://doi.org/10.2307/1351691

Goncalves, J.A., Henriques, R., 2015. UAV photogrammetry for topographic monitoring of coastal areas. ISPRS J. Photogramm. Remote Sens. 104, 101–111. https://doi.org/10.1016/j.isprsjprs.2015.02.009

Gronewold, A.D., Bruxer, J., Durnford, D., Smith, J.P., Clites, A.H., Seglenieks, F., Qian, S.S., Hunter, T.S., Fortin, V., 2016. Hydrological drivers of record-setting water level rise on Earth's largest lake system. Water Resour. Res. 52, 4026–4042. https://doi.org/10.1002/2015WR018209

Larsen, C.E., 1985. A stratigraphic study of beach features on the southwestern shore of Lake Michigan: new evidence of Holocene lake level fluctuations. Environ. Geol. Notes - Illinois State Geol. Surv.

112.
Lee, J., Hopmans, J.W., Rolston, D.E., Baer, S.G., Six, J., 2009. Determining soil carbon stock changes: Simple bulk density corrections fail. Agric. Ecosyst. Environ. 134, 251–256. https://doi.org/10.1016/j.agee.2009.07.006
Meadows, G.A., Meadows, L.A., Wood, W.L., Hubertz, J.M., Perlin, M., 1997. The Relationship between Great Lakes Water Levels, Wave Energies, and Shoreline Damage. Bull. Am. Meteorol. Soc. 78, 675–683. https://doi.org/http://dx.doi.org/10.1175/1520-0477(1997)078<0675:TRBGLW>2.0.CO;2
National Oceanic and Atmospheric Administration Great Lakes Environmental Research Laboratory (2019). Great Lakes Coastal Forecasting System, Lake Michigan [NOWCAST and FORECAST]. Dataset. https://www.glerl.noaa.gov/res/glcfs/. Accessed February 4, 2020.
Quinn, F.H., 2002. Secular changes in Great Lakes water level seasonal cycles. J. Great Lakes Res. 28, 451–465. https://doi.org/10.1016/S0380-1330(02)70597-2
Redfield, A.C., Rubin, M., 1962. The age of salt marsh peat and its relation to recent changes in sea level at Barnstable, Massachusetts. Proc. Natl. Acad. Sci. U. S. A. 48, 1728–1735. https://doi.org/10.1073/pnas.48.10.1728
Reimer, P.J., Bard, E., Bayliss, A., Beck, J.W., Blackwell, P.G., Ramsey, C.B., Buck, C.E., Cheng, H., Edwards, R.L., Friedrich, M., Grootes, P.M., Guilderson, T.P., Haflidason, H., Hajdas, I., Hatté, C., Heaton, T.J., Hoffmann, D.L., Hogg, A.G., Hughen, K.A., Kaiser, K.F., Kromer, B., Manning, S.W., Niu, M., Reimer, R.W., Richards, D.A., Scott, E.M., Southon, J.R., Staff, R.A., Turney, C.S.M., van der Plicht, J., 2013. IntCal13 and Marine13 Radiocarbon Age Calibration Curves 0–50,000 Years cal BP. Radiocarbon 55, 1869–1887. https://doi.org/10.2458/azu_js_rc.55.16947
Smeaton, C., Barlow, N.L.M., Austin, W.E.N., 2020. Coring and compaction: Best practice in blue carbon stock and burial estimations. Geoderma 364, 114180. https://doi.org/10.1016/j.geoderma.2020.114180
Theuerkauf, E.J., Braun, K.N., Kaplan, M., Vivirito, S., Williams, J.D., Nelson, D.M., 2019. Coastal Geomorphic Response to Seasonal Lake Level Rise in the Laurentian Great Lakes, USA. J. Great Lakes Res. 45, 1055–1068. https://doi.org/10.1016/j.jglr.2019.09.012
Theuerkauf, E.J., Stephens, J.D., Ridge, J.T., Fodrie, F.J., Rodriguez, A.B., 2015. Carbon export from fringing saltmarsh shoreline erosion overwhelms carbon storage across a critical width threshold. Estuar. Coast. Shelf Sci. 164, 367–378. https://doi.org/10.1016/j.ecss.2015.08.001
Thompson, T.A., 1992. Beach-ridge development and lake-level variation in southern Lake Michigan. Sediment. Geol. 80, 305–318. https://doi.org/10.1016/0037-0738(92)90048-V
Thompson, T.A., Baedke, S.J., 1997. Strand-plain evidence for late Holocene lake-level variations in Lake Michigan. Bull. Geol. Soc. Am. 109, 666–682. https://doi.org/10.1130/0016-7606(1997)109<0666:SPEFLH>2.3.CO;2
Turner, I.L., Harley, M.D., Drummond, C.D., 2016. UAVs for coastal surveying. Coast. Eng. 114, 19–24. https://doi.org/10.1016/j.coastaleng.2016.03.011
Walter, K., Don, A., Tiemeyer, B., Freibauer, A., 2016. Determining Soil Bulk Density for Carbon Stock Calculations: A Systematic Method Comparison. Soil Sci. Soc. Am. J. 80, 579–591. https://doi.org/10.2136/sssaj2015.11.0407